

Part One

Fuel Cells

1

The Direct Ethanol Fuel Cell: a Challenge to Convert Bioethanol Cleanly into Electric Energy

Claude Lamy, Christophe Coutanceau, and Jean-Michel Leger

1.1

Introduction

Discovered in England in 1839 by Sir William Grove, a fuel cell (FC) is an electrochemical device which transforms directly the heat of combustion of a fuel (hydrogen, natural gas, methanol, ethanol, hydrocarbons, etc.) into electricity [1]. The fuel is electrochemically oxidized at the anode, without producing any pollutants (only water and/or carbon dioxide are released into the atmosphere), whereas the oxidant (oxygen from the air) is reduced at the cathode. This process does not follow Carnot's theorem, so that higher energy efficiencies are expected: 40–50% in electrical energy, 80–85% in total energy (electricity + heat production).

There is now a great interest in developing different kinds of fuel cells with several applications (in addition to the first and most developed application in space programs) depending on their nominal power: stationary electric power plants (100 kW–10 MW), power train sources (20–200 kW) for the electrical vehicle (bus, truck and individual car), electricity and heat co-generation for buildings and houses (5–20 kW), auxiliary power units (1–100 kW) for different uses (automobiles, aircraft, space launchers, space stations, uninterruptible power supply, remote power, etc.) and portable electronic devices (1–100 W), for example, cell phones, computers, camcorders [2, 3].

For many applications, hydrogen is the most convenient fuel, but it is not a primary fuel, so that it has to be produced from different sources: water, fossil fuels (natural gas, hydrocarbons, etc.), biomass resources and so on. Moreover, the clean production of hydrogen (including the limitation of carbon dioxide production) and the difficulties with its storage and large-scale distribution are still strong limitations for the development of such techniques [2, 3]. In this context, other fuels, particularly those, like alcohols, which are liquid at ambient temperature and pressure, are more convenient due to the ease of their handling and distribution.

Therefore, alcohols have begun to be considered as valuable alternative fuels, because they have a high energy density (6–9 kW h kg⁻¹, compared with 33 kW h kg⁻¹

for pure hydrogen without a storage tank and about 11 kW h kg^{-1} for gasoline) and they can be obtained from renewable sources (e.g. bioethanol from biomass feedstock). Ethanol is an attractive fuel for electric vehicles, since it can be easily produced in great quantities by the fermentation of cellulose-containing raw materials from agriculture (corn, wheat, sugar beet, sugar cane, etc.) or from different wastes (e.g. agricultural wastes containing lignocellulosic residues). In addition, in some countries such as Brazil and the USA and more recently in France (with the E85 fuel containing 85% of ethanol), ethanol is already distributed through the fuel station network for use in conventional automobiles with internal combustion engines (flex-fuel vehicles). Moreover, for portable electronics, particularly cell phones, ethanol can advantageously replace methanol, which is used in the direct methanol fuel cell (DMFC), since it is less toxic and has better energy density and similar kinetics at low temperature.

DMFCs and direct ethanol fuel cells (DEFCs) are based on the proton exchange membrane fuel cell (PEMFC), where hydrogen is replaced by the alcohol, so that both the principles of the PEMFC and the direct alcohol fuel cell (DAFC), in which the alcohol reacts directly at the fuel cell anode without any reforming process, will be discussed in this chapter. Then, because of the low operating temperatures of these fuel cells working in an acidic environment (due to the protonic membrane), the activation of the alcohol oxidation by convenient catalysts (usually containing platinum) is still a severe problem, which will be discussed in the context of electrocatalysis. One way to overcome this problem is to use an alkaline membrane (conducting, e.g., by the hydroxyl anion, OH^-), in which medium the kinetics of the electrochemical reactions involved are faster than in an acidic medium, and then to develop the solid alkaline membrane fuel cell (SAMFC).

After rehearsing the working principles and presenting the different kinds of fuel cells, the proton exchange membrane fuel cell (PEMFC), which can operate from ambient temperature to $70\text{--}80^\circ\text{C}$, and the direct ethanol fuel cell (DEFC), which has to work at higher temperatures (up to $120\text{--}150^\circ\text{C}$) to improve its electric performance, will be particularly discussed. Finally, the solid alkaline membrane fuel cell (SAMFC) will be presented in more detail, including the electrochemical reactions involved.

1.2 Principles and Different Kinds of Fuel Cells

1.2.1 Working Principles of a Fuel Cell

The principles of the fuel cell are illustrated in Figure 1.1. The electrochemical cell consists of two electrodes, an anode and a cathode, which are electron conductors, separated by an electrolyte [e.g. a proton exchange membrane (PEM) in a PEMFC or in a DAFC], which is an ion conductor (as the result of proton migration and diffusion inside the PEM). An elementary electrochemical cell converts directly the chemical

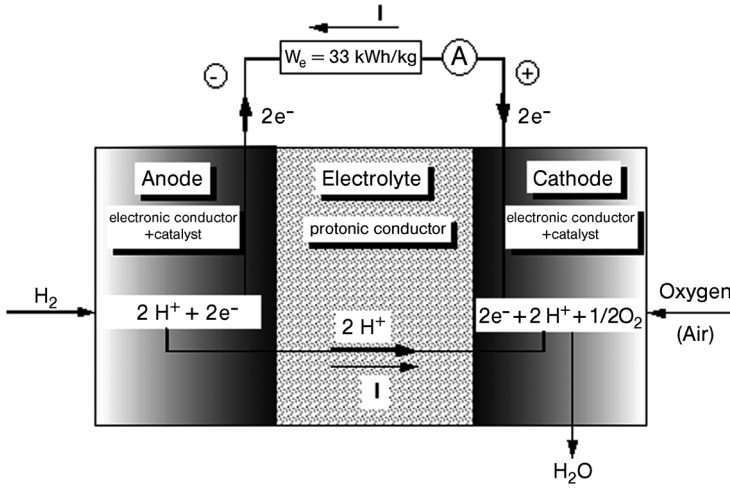


Figure 1.1 Schematic diagram of a hydrogen/oxygen fuel cell.

energy of combustion in oxygen (i.e. the Gibbs free energy change, $-\Delta G$) of a given fuel (hydrogen, natural gas, hydrocarbons, kerosene, alcohols, biomass resources and wastes) into electricity [4–8].

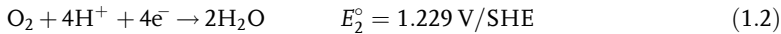
Electrons liberated at the anode (negative pole of the cell) by the electro-oxidation of the fuel pass through the external circuit (producing electric energy equal to $-\Delta G$) and arrive at the cathode (positive pole), where they reduce oxygen (from air). Inside the fuel cell, the electric current is transported by migration and diffusion of the electrolyte ions (H^+ , OH^- , O^{2-} , CO_3^{2-}), for example, H^+ in a PEMFC.

1.2.1.1 The Thermodynamics of Fuel Cells

At the anode, the electro-oxidation of hydrogen takes place as follows:



whereas the cathode undergoes the electro-reduction of oxygen:



where E_i° are the standard electrode potentials versus the standard hydrogen (reference) electrode (SHE). The standard cell voltage is thus $E_{\text{eq}}^\circ = E_2^\circ - E_1^\circ = 1.229 \text{ V} \approx 1.23 \text{ V}$. This corresponds to the overall combustion reaction of hydrogen in oxygen:



with the following thermodynamic data, under standard conditions: $\Delta G^\circ = -237 \text{ kJ mol}^{-1}$; $\Delta H^\circ = -286 \text{ kJ mol}^{-1}$ of H_2 .

The protons produced at the anode cross over the membrane, ensuring the electrical conductivity inside the electrolyte, whereas the electrons liberated at

the anode reach the cathode (where they reduce oxygen) through the external circuit. This process produces an electric energy, $W_{el} = nFE_{eq}^{\circ} = -\Delta G^{\circ}$, corresponding to an energy mass density of the fuel $W_e = -\Delta G^{\circ}/(3600M) = 32.9 \text{ kW h kg}^{-1} \approx 33 \text{ kW h kg}^{-1}$, where $M = 0.002 \text{ kg}$ is the molecular weight of hydrogen, $F = 96485 \text{ C}$ the Faraday constant (i.e. the absolute value of the electric charge of 1 mol of electrons) and $n=2$ the number of electrons involved in the oxidation of one hydrogen molecule.

The standard electromotive force (emf), E_{eq}° , at equilibrium (no current flowing) under standard conditions is then calculated as follows:

$$E_{eq}^{\circ} = -\frac{\Delta G^{\circ}}{nF} = \frac{237 \times 10^3}{2 \times 96485} = E_2^{\circ} - E_1^{\circ} = 1.229 \text{ V} \approx 1.23 \text{ V} \quad (1.4)$$

The working of the cell under reversible thermodynamic conditions does not follow Carnot's theorem, so that the theoretical energy efficiency, $\epsilon_{cell}^{\text{rev}}$, defined as the ratio between the electrical energy produced ($-\Delta G^{\circ}$) and the heat of combustion ($-\Delta H^{\circ}$) at constant pressure, is

$$\epsilon_{cell}^{\text{rev}} = \frac{W_e}{-\Delta H^{\circ}} = \frac{nFE_{eq}^{\circ}}{-\Delta H^{\circ}} = \frac{\Delta G^{\circ}}{\Delta H^{\circ}} = 1 - \frac{T\Delta S^{\circ}}{\Delta H^{\circ}} = \frac{237}{286} = 0.83 \quad (1.5)$$

for the hydrogen/oxygen fuel cell at 25 °C.

This theoretical efficiency is much greater (by a factor of about 2) than that of a thermal combustion engine, producing the reversible work, W_r , according to Carnot's theorem:

$$\epsilon_{\text{therm}}^{\text{rev}} = \frac{W_r}{-\Delta H^{\circ}} = \frac{Q_1 - Q_2}{Q_1} = 1 - \frac{Q_2}{Q_1} = 1 - \frac{T_2}{T_1} = 0.43 \quad (1.6)$$

for, for example, $T_1 = 350 \text{ }^{\circ}\text{C}$ and $T_2 = 80 \text{ }^{\circ}\text{C}$, where Q_1 and Q_2 are the heat exchanged with the hot source and cold source, respectively.

1.2.1.2 The Kinetics of Fuel Cells

However, under working conditions, with a current density j , the cell voltage $E(j)$ becomes smaller than the equilibrium cell voltage E_{eq} , as the result of three limiting factors: (i) the overvoltages η_a and η_c at both electrodes due to a rather low reaction rate of the electrochemical reactions involved (η is defined as the difference between the working electrode potential E_i and the equilibrium potential E_i^{eq} , so that $E_i = E_i^{\text{eq}} + \eta$), (ii) the ohmic drop $R_e j$ both in the electrolyte and interface resistances R_e and (iii) mass transfer limitations for reactants and products (Figure 1.2).

The cell voltage, $E(j)$, defined as the difference between the cathode potential E_2 and the anode potential E_1 , can thus be expressed as

$$\begin{aligned} E(|j|) &= E_2(|j|) - E_1(|j|) = E_2^{\text{eq}} + \eta_c - (E_1^{\text{eq}} + \eta_a) - R_e |j| \\ &= E_{eq} - (|\eta_a| + |\eta_c| + R_e |j|) \end{aligned} \quad (1.7)$$

where the overvoltages η_a (anodic reaction, i.e. oxidation of the fuel with $\eta_a > 0$) and η_c (cathodic reaction, i.e. reduction of the oxidant with $\eta_c < 0$) take into account both the

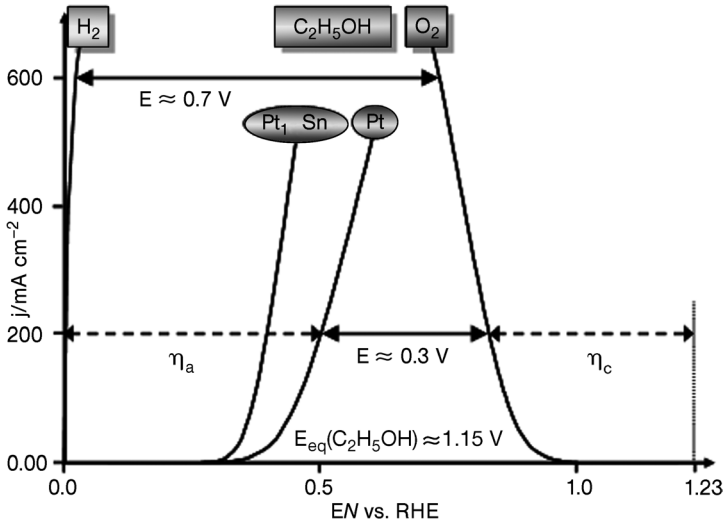


Figure 1.2 Comparative current density (j) vs potential (E) curves for H_2 and EtOH electro-oxidation at different Pt-based catalytic anodes and oxygen electro-reduction at a Pt cathode.

low kinetics of the electrochemical reactions involved (charge transfer overvoltage or activation polarization) and the limiting rate of mass transfer (mass transfer overvoltage or concentration polarization) – see Figure 1.3.

In the $E(j)$ characteristics one may distinguish three zones associated with these energy losses:

- *Zone I:* the E vs j linear curve corresponds to ohmic losses $R_e |j|$ in the electrolyte and interface resistances; a decrease of the specific electric resistance R_e from 0.3 to $0.15 \Omega \text{ cm}^2$ gives an increase in the current density j (at 0.7 V) from 0.25 to 0.4 A cm^{-2} , that is, an increase in the energy efficiency and in the power density of 1.6-fold.
- *Zone II:* the E vs $\ln(|j|/j_0)$ logarithmic curve corresponds to the charge transfer polarization, that is, to the activation overvoltages due to a relatively low electron exchange rate at the electrode–electrolyte interface, particularly for the oxygen reduction reaction whose exchange current density j_0 is much smaller than that of the hydrogen oxidation; an increase in j_0 from 10^{-8} to $10^{-6} \text{ A cm}^{-2}$ leads to an increase in the current density j (at 0.7 V) from 0.4 to 0.9 A cm^{-2} , that is, an increase in the energy efficiency and in the power density of 3.6-fold compared with the initial data.
- *Zone III:* the E vs $\ln(1 - |j|/j_l)$ logarithmic curve corresponds to concentration polarization, which results from the limiting value j_l of the mass transfer limiting current density for the reactive species and reaction products to and/or from the electrode active sites; an increase in j_l from 1.4 to 2.2 A cm^{-2} leads to a further

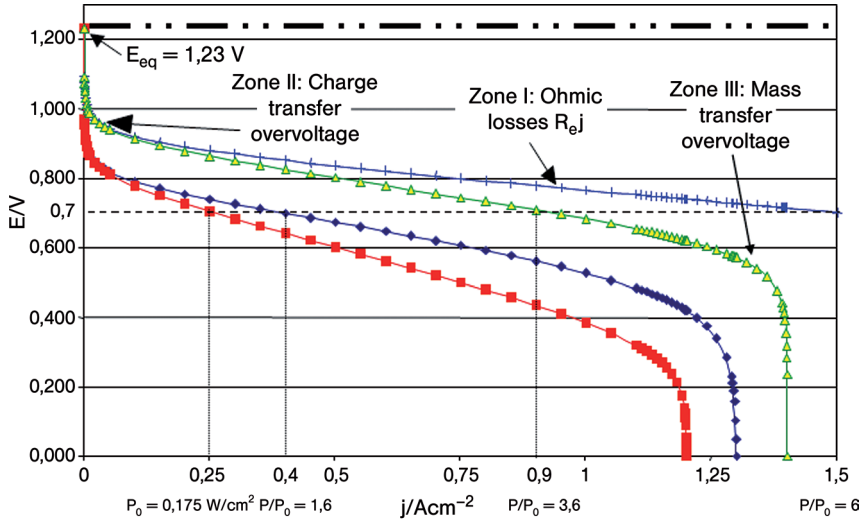


Figure 1.3 Theoretical $E(j)$ electric characteristics of an H_2/O_2 fuel cell: (■) $j_0 = 10^{-8} \text{ A cm}^{-2}$, $R_e = 0.30 \Omega \text{ cm}^2$, $j_i = 1.2 \text{ A cm}^{-2}$; (◆) $j_0 = 10^{-8}$, $R_e = 0.15$, $j_i = 1.3$; (△) $j_0 = 10^{-6}$, $R_e = 0.15$, $j_i = 1.4$; (+) $j_0 = 10^{-6}$, $R_e = 0.10$, $j_i = 2.2$.

increase in the current density j (at 0.7 V) from 0.9 to 1.5 A cm^{-2} , that is, an increase in the energy efficiency and in the power density of 6-fold compared with the initial curve.

Hence these three key points will determine the energy efficiency and the specific power of the elementary fuel cell: an improvement in each component of the cell will increase the power density from 0.175 to 1.05 W cm^{-2} , that is, an increase by a factor of 6. As a consequence, for the fuel cell systems the weight and volume will be decreased by a similar factor, for a given power of the system, and presumably the overall cost will be diminished. The improvement in the components of the elementary fuel cell thus has a direct effect on the system technology and therefore on the overall cost.

For a PEMFC, fed with reformat hydrogen and air, the working cell voltage is typically 0.8 V at 500 mA cm^{-2} , which leads to a voltage efficiency ϵ_E given by

$$\epsilon_E = \frac{E(j)}{E_{\text{eq}}^{\circ}} = 1 - \frac{|\eta_a(j)| + |\eta_c(j)| + R_e |j|}{E_{\text{eq}}^{\circ}} = \frac{0.8}{1.23} = 0.65 \quad (1.8)$$

The overall energy efficiency (ϵ_{cell}) thus becomes

$$\epsilon_{\text{cell}} = \frac{W_{\text{el}}}{-\Delta H^{\circ}} = \frac{n_{\text{exp}} F E(|j|)}{-\Delta H^{\circ}} = \frac{n_{\text{exp}}}{n_{\text{th}}} \frac{E(|j|)}{E_{\text{eq}}^{\circ}} \frac{n_{\text{th}} F E_{\text{eq}}^{\circ}}{-\Delta H^{\circ}} = \epsilon_F \epsilon_E \epsilon_{\text{cell}}^{\text{rev}} \quad (1.9)$$

where the faradaic efficiency $\epsilon_F = n_{\text{exp}}/n_{\text{th}}$ is the ratio between the number of electrons n_{exp} effectively exchanged in the overall reaction and the theoretical

numbers of electrons n_{th} for complete oxidation of the fuel (to H_2O and CO_2). $\epsilon_F = 1$ for hydrogen oxidation, but $\epsilon_F = 4/12 = 0.33$ for ethanol oxidation stopping at the acetic acid stage (four electrons exchanged instead of 12 electrons for complete oxidation to CO_2) – see Section 1.3.2.1.

As an example, the overall energy efficiency of an H_2/O_2 fuel cell, working at 0.8 V under 500 mA cm^{-2} , is

$$\epsilon_{\text{cell}}^{\text{H}_2/\text{O}_2} = 1 \times 0.65 \times 0.83 = 0.54 \quad (1.10)$$

whereas that of a DEFC working at 0.5 V under 100 mA cm^{-2} (assuming complete oxidation to CO_2) would be

$$\begin{aligned} \epsilon_{\text{cell}}^{\text{C}_2\text{H}_5\text{OH}/\text{O}_2} &= 1 \times 0.44 \times 0.97 = 0.43 \text{ since } \epsilon_F = 1, \\ \epsilon_E &= \frac{0.5}{1.14} = 0.44 \text{ and } \epsilon_{\text{cell}}^{\text{rev}} = \frac{1325}{1366} = 0.97 \end{aligned} \quad (1.11)$$

with $\Delta G^\circ = -1325 \text{ kJ mol}^{-1}$, $E_{\text{eq}}^\circ = (1325 \times 10^3)/(12 \times 96485) = 1.144 \text{ V}$ and $\Delta H^\circ = -1366 \text{ kJ mol}^{-1}$ of ethanol (see Section 1.3.2.1).

These energy efficiencies are better than those of the best thermal engines (diesel engines), which have energy efficiency of the order of 0.40.

Therefore, it appears that the only way to increase significantly the overall energy efficiency is to increase ϵ_E and ϵ_F , that is, to decrease the overvoltages η and the ohmic drop $R_{\Omega}j$ and to increase the faradaic efficiency for complete oxidation, since $\epsilon_{\text{cell}}^{\text{rev}}$ is given by the thermodynamics (one can increase it slightly by changing the pressure and temperature operating conditions). For the hydrogen/oxygen fuel cell, usually $\epsilon_F \approx 1$, but it can be much lower in the case of incomplete combustion of the fuel (see, e.g., the case of the DEFC in Section 1.3.2.1). The decrease in $|\eta|$ is directly related to the increase in the rate of the electrochemical reactions occurring at both electrodes. This is typically the field of electrocatalysis, where the action of both the electrode potential and the catalytic electrode material will synergistically increase the reaction rate ν [9–11].

1.2.1.3 Catalysis of Fuel Cell Reactions

Electrocatalysis and the Rate of Electrochemical Reactions For a given electrochemical reaction $\text{A} + n\text{e}^- \rightleftharpoons \text{B}$, which involves the transfer of n electrons at the electrode/electrolyte interface, the equilibrium potential, called the electrode potential, is given by the Nernst law:

$$E_{\text{eq}}^{\text{A/B}} = E_0^{\text{A/B}} + \frac{RT}{nF} \ln \frac{a_{\text{A}}}{a_{\text{B}}} \quad (1.12)$$

where $E_0^{\text{A/B}}$ is the standard electrode potential, as measured versus the standard hydrogen electrode (SHE), the potential of which is zero at 25 °C by definition, and a_i is the activity of reactant i .

As soon as the electrode potential takes a value $E^{\text{A/B}}$ different from the equilibrium potential $E_{\text{eq}}^{\text{A/B}}$, an electrical current of intensity I passes through the interface, the magnitude of which depends on the deviation $\eta = E^{\text{A/B}} - E_{\text{eq}}^{\text{A/B}}$ from the equilibrium

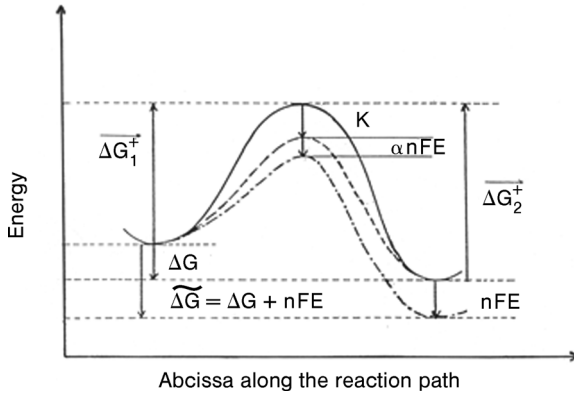


Figure 1.4 Activation barrier for an electrochemical reaction. K is the decrease in activation energy due to the electrode catalyst and αnFE is that due to the electrode potential E .

potential. η , which is called the overvoltage, is positive for an oxidation reaction (anodic reaction $B \rightarrow A + ne^-$) and negative for a reduction reaction (cathodic reaction $A + ne^- \rightarrow B$). The current intensity I is proportional to the rate of reaction v , that is, $I = nFv$. For heterogeneous reaction v is proportional to the surface area S of the interface, so that the kinetics of electrochemical reactions are better defined by the intrinsic rate $v_i = v/S$ and the current density $j = I/S = nFv_i$.

The electrical characteristics $j(E)$ can then be obtained by introducing the exponential behavior of the rate constant with the electrochemical activation energy, $\hat{\Delta G}^+ = \Delta G_0^+ - \alpha nFE$, which comprises two terms: the first (ΔG_0^+) is the chemical activation energy and the second (αnFE) is the electrical part of the activation energy. This latter is a fraction α ($0 \leq \alpha \leq 1$) of the total electric energy, nFE , coming from the applied electrode potential E , where α is called the charge transfer coefficient (Figure 1.4). In the theory of absolute reaction rate, one obtains, for a first-order electrochemical reaction (the rate of which is proportional to the reactant concentration c_i):

$$\begin{aligned} j &= nFv_i = nFk(T, E)c_i = nFk_0c_i e^{-(\hat{\Delta G}^+/RT)} \\ &= nFk_0c_i e^{-(\Delta G_0^+/RT)} e^{(\alpha nFE/RT)} = j_0 e^{(\alpha nFE/RT)} \end{aligned} \quad (1.13)$$

This equation contains the two essential activation terms met in electrocatalysis: (i) an exponential function of the electrode potential E and (ii) an exponential function of the chemical activation energy ΔG_0^+ . By modifying the nature and structure of the electrode material, one may decrease ΔG_0^+ , by a given amount K (see Figure 1.4), thus increasing j_0 , as the result of the catalytic properties of the electrode. This leads to an increase of the reaction rate v_i , that is, the current density j .

Electrocatalytic Oxidation of Hydrogen The rate constant of the hydrogen oxidation reaction (HOR), as measured by the exchange current density j_0 (i.e. the current

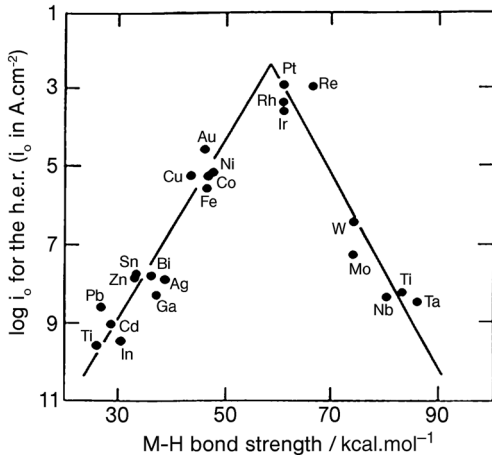
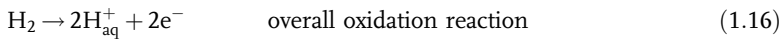
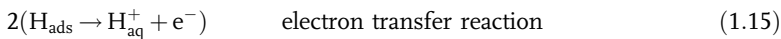
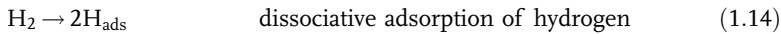


Figure 1.5 Exchange current density of the hydrogen reaction as a function of the metal–hydrogen bond energy [12].

density at the equilibrium potential $E_{\text{eq}}^{A/B}$, where the anodic current is exactly compensated by the cathodic current, so that the overall current is zero) depends greatly on the electrode material (Figure 1.5).

These values can be correlated with the heat of adsorption of hydrogen on the catalytic metal since the oxidation mechanism, apart from diffusion and mass transport limitations, is controlled by an adsorption step in a two consecutive step mechanism:



where H_{aq}^+ is a proton solvated by the electrolytic medium (usually an aqueous electrolyte). This leads to a Volcano plot (Figure 1.5) with a maximum of activity for the transition noble metals (Pt, Pd, Rh).

Oxidation of Alcohols in a Direct Alcohol Fuel Cell The electrocatalytic oxidation of an alcohol (methanol, ethanol, etc.) in a direct alcohol fuel cell (DAFC) will avoid the presence of a heavy and bulky reformer, which is particularly convenient for applications to transportation and portable electronics. However, the reaction mechanism of alcohol oxidation is much more complicated, involving multi-electron transfer with many steps and reaction intermediates. As an example, the complete oxidation of methanol to carbon dioxide:



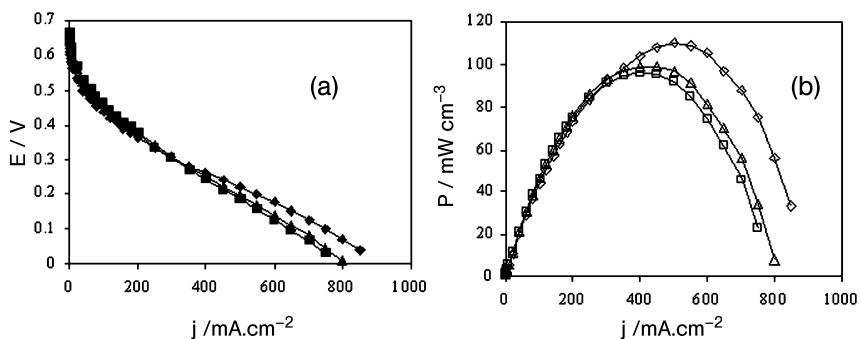
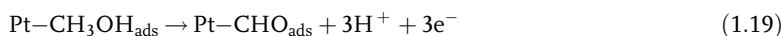


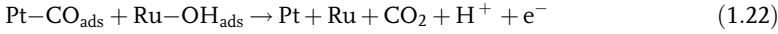
Figure 1.6 (a) $E(j)$ and (b) $P(j)$ curves at 110°C of a DMFC with different Pt/Ru atomic ratios in the anode catalyst (■, 50 : 50; ▲, 70 : 30; ◆, 80 : 20).

involves the transfer of six electrons and the formation of many adsorbed species and reaction intermediates, among them adsorbed CO, which blocks the active sites of platinum catalysts. As a result of such a complex reaction, the oxidation overvoltage η_a is relatively high (0.3–0.5 V), so that more effective electrocatalysts are needed in order to increase the reaction rate and thus to decrease η_a . Therefore, several bi- and trimetallic catalysts were developed, among which Pt/Ru-based electrocatalysts lead to the best performance.

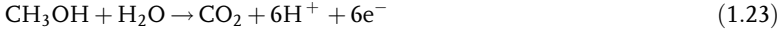
Pt/Ru electrocatalysts are currently used in DMFC stacks of a few watts to a few kilowatts. The atomic ratio between Pt and Ru, the particle size and the metal loading of carbon-supported anodes play a key role in their electrocatalytic behavior. Commercial electrocatalysts (e.g. from E-Tek) consist of 1 : 1 Pt/Ru catalysts dispersed on an electron-conducting substrate, for example carbon powder such as Vulcan XC72 (specific surface area of $200\text{--}250\text{ m}^2\text{ g}^{-1}$). However, fundamental studies carried out in our laboratory [13] showed that a 4 : 1 Pt/Ru ratio gives higher current and power densities (Figure 1.6).

This may be explained by the bifunctional theory of electrocatalysis developed by Watanabe and Motoo [14], according to which Pt activates the dissociative chemisorption of methanol to CO, whereas Ru activates and dissociates water molecules, leading to adsorbed hydroxyl species, OH. A surface oxidation reaction between adsorbed CO and adsorbed OH becomes the rate-determining step. The reaction mechanism can be written as follows [15]:





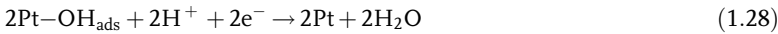
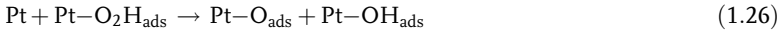
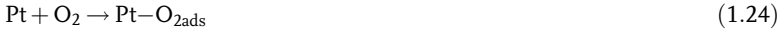
Overall reaction:



In this reaction mechanism, three or four Pt sites are involved in methanol dissociation, whereas only one Ru site is involved in water activation, so that the best Pt/Ru atomic ratio is between 3 : 1 and 4 : 1 [15].

Some Pt/Ru-based trimetallic electrocatalysts, such as Pt/Ru/Mo, give enhanced catalytic activity leading to a power density, in an elementary single DMFC, at least twice that of Pt/Ru catalyst.

Electrocatalytic Reduction of Dioxygen The electrocatalytic reduction of oxygen is another multi-electron transfer reaction (four electrons are involved) with several steps and intermediate species [16]. A four-electron mechanism, leading to water, is in competition with a two-electron mechanism, giving hydrogen peroxide. The four-electron mechanism on a Pt electrode can be written as follows:



Overall reaction:



This complex reduction reaction leads to a relatively high overvoltage – at least 0.3 V – thus decreasing the cell voltage of the fuel cell by the same quantity. Pt-X binary catalysts (with X = Cr, Ni, Fe, ...) give some improvements in the electrocatalytic properties compared with pure Pt dispersed on Vulcan XC72 [17].

In addition, in a DAFC, the proton exchange membrane is not completely alcohol tight, so that some alcohol leakage to the cathodic compartment will lead to a mixed potential with the oxygen electrode. This mixed potential will decrease further the cell voltage by about 0.1–0.2 V. It turns out that new electrocatalysts insensitive to the presence of alcohols are needed for the DAFC.

Transition metal compounds, such as organic macrocycles, are known to be good electrocatalysts for oxygen reduction. Furthermore, they are inactive for alcohol oxidation. Different phthalocyanines and porphyrins of iron and cobalt were thus dispersed in an electron-conducting polymer (polyaniline, polypyrrole) acting as a conducting matrix, either in the form of a tetrasulfonated counter anion or linked to

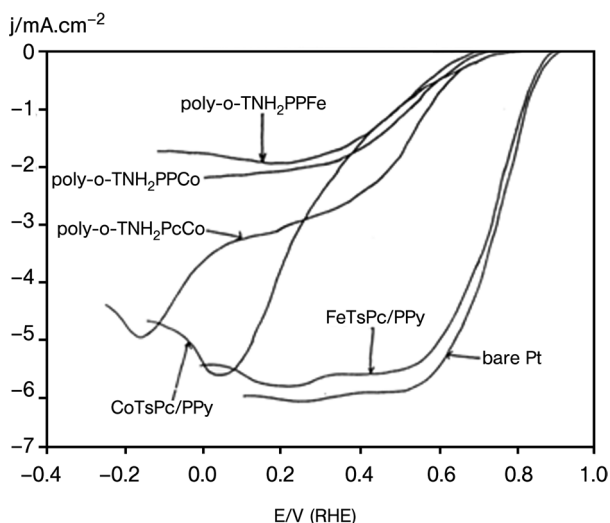


Figure 1.7 Activity of different electrodes containing macrocycles for the oxygen reduction reaction.

the monomer before its electro-polymerization. Among the different macrocyclic compounds investigated in our laboratory, tetrasulfonated iron phthalocyanine (FeTsPc), incorporated in polypyrrole, has a catalytic activity close to that of pure platinum (Figure 1.7).

However, the stability with time and/or temperature of these modified electrodes needs to be greatly improved for practical applications (except maybe for power sources in portable electronics working at room temperature).

Further, Pt-based binary catalysts, such as Pt/Cr and Pt/Ni [18], are less sensitive to the presence of alcohol than pure Pt, giving hope for the development of better catalysts for oxygen reduction.

1.2.2

Different Types of Fuel Cells

Different types of fuel cells have been developed and are classified mainly according to (i) the type of fuel, (ii) the operating temperature range and/or electrolyte or (iii) the direct or indirect utilization of fuel [19]. The state-of-the-art and the different applications of fuel cells are summarized in Table 1.1.

1.2.2.1 Fuels for Fuel Cells

For fuel cells operating at low (<100 °C) and intermediate temperatures (up to 200 °C), H₂ and H₂-CO₂ (with minimal amounts of CO) are the ideal fuels. The H₂-CO₂ gas mixture is produced by steam reforming/water gas shift conversion or partial oxidation/water gas shift conversion of primary or secondary organic fuels. On a large scale, hydrogen is produced from the primary fuels, that is, natural gas, oil or coal gasification, but it can be generated by water electrolysis using nuclear power plants, avoiding the direct production of CO₂ and CO.

Table 1.1 Status of fuel cell technologies.

Type of fuel cell ^a ; operating fuel and temperature	Power rating (kW)	Fuel efficiency (%)	Power density (mW cm ⁻²)	Lifetime (h)	Capital cost (\$ kW ⁻¹)	Applications
SOFC; CH ₄ , coal [?] , 800–1000 °C	25–5000	50–60	200–400	8000–40 000	1500	Base-load and intermediate load, power generation, co-generation
MCFC; CH ₄ , coal [?] , 650 °C	100–5000	50–55	150–300	10 000–40 000	1250	Base-load and intermediate load, power generation – co-generation
PAFC; CH ₄ , CH ₃ OH, oil, 200 °C	200–10 000	40–45	200–300	30 000–40 000	200–3000	On-site integrated energy systems, transportation (fleet vehicles), load-leveling
AFC; H ₂ , 80 °C	20–100	65	250–400	3000–10 000	1000	Space flights, space stations, transportation, APU
PEMFC; H ₂ , CH ₃ OH, 25–100 °C	0.01–250	40–50	500–1000	10 000–100 000	50–2000	Transportation, stand-by power, portable power, space stations
DMFC; CH ₃ OH, 25–150 °C	0.001–10	30–45	50–200	1000–10 000	1000	Portable power, stand-by power, transportation (?), APU
SAMFC; H ₂ , CH ₃ OH, C ₂ H ₅ OH, NaBH ₄ , 25–80 °C	0.001–0.1	30–60	10–100	?	?	Portable power

^aSOFC = solid oxide fuel cell; MCFC = molten carbonate fuel cell; PAFC = phosphoric acid fuel cell; AFC = alkaline fuel cell; PEMFC = proton exchange membrane fuel cell; DMFC = direct methanol fuel cell; SAMFC = Solid alkaline membrane fuel cell.

These fuels (pure H_2 , H_2-CO_2 , $H_2-CO-CO_2$) may also be produced from renewable energy sources, such as biomass, solar, windmill and hydroelectric power.

Hydrogen is a secondary fuel and, like electricity, is an energy carrier. It is the most electroactive fuel for fuel cells operating at low and intermediate temperatures. Methanol and ethanol are the most electroactive alcohol fuels, and, when they are electro-oxidized directly at the fuel cell anode (instead of being transformed in a hydrogen-rich gas in a fuel processor), the fuel cell is called a DAFC: either a DMFC (with methanol) or a DEFC (with ethanol).

1.2.2.2 Hydrogen-fed Fuel Cells

Hydrogen/oxygen (air) fuel cells are classified according to the type of electrolyte used and the working temperature:

- Solid oxide fuel cell (SOFC) working between 700 and 1000 °C with a solid oxide electrolyte, such as yttria-stabilized zirconia ($ZrO_2-8\% Y_2O_3$), conducting by the O^{2-} anion.
- Molten carbonate fuel cell (MCFC) working at about 650 °C with a mixture of molten carbonates ($Li_2CO_3-K_2CO_3$) as electrolyte, conducting by the CO_3^{2-} anion.

Both of the above are high-temperature fuel cells.

- Phosphoric acid fuel cell (PAFC) working at 180–200 °C with a porous matrix of PTFE-bonded silicon carbide impregnated with phosphoric acid as electrolyte, conducting by the H^+ cation. This medium-temperature fuel cell is now commercialized by ONSI (USA), mainly for stationary applications.
- Alkaline fuel cell (AFC) working at 80 °C with concentrated potassium hydroxide as electrolyte, conducting by the OH^- anion. This kind of fuel cell, developed by IFC (USA), is now used in space shuttles.
- Proton exchange membrane fuel cell (PEMFC) working at around 70 °C with a polymer membrane electrolyte, such as Nafion, which is a solid proton conductor (conducting by the H^+ cation).
- Direct methanol fuel cell (DMFC) working between 30 and 110 °C with a proton exchange membrane (such as Nafion) as electrolyte, which realizes the direct oxidation of methanol at the anode.
- Solid alkaline membrane fuel cell (SAMFC) working at moderate temperatures (20–80 °C) for which an anion-exchange membrane (AEM) is the electrolyte, electrically conducting by, for example, hydroxyl ions (OH^-).

1.2.2.3 Methanol- and Ethanol-fed Fuel Cells

In addition to hydrogen as a fuel, methanol or ethanol can be directly converted into electricity in a DAFC, the great progress of which resulted from the use of a proton exchange membrane acting both as an electrolyte (instead of the aqueous electrolytes previously used) and as a separator preventing the mixing of fuel and oxidant. A DAFC can work at moderate temperatures (30–50 °C) for portable applications, but now the tendency is to look for new membranes that are less permeable to alcohol and

work at higher temperatures (80–120 °C) to increase the rate of the electrochemical reactions involved (oxidation of alcohol and reduction of oxygen) and to manage better the heat produced, either to use it in a co-generation system or to evacuate it in transportation applications.

The last three fuel cells (PEMFC, DAFC and SAMFC) are low-temperature fuel cells. In this chapter, the discussion will be focused on these fuel cells, particularly the PEMFC and the DAFC, since they can accommodate biomass fuels, either after fuel processing to obtain reformat hydrogen or directly with bioethanol.

For these low-temperature fuel cells, the development of catalytic materials is essential to activate the electrochemical reactions involved. This concerns the electro-oxidation of the fuel (reformat hydrogen containing some traces of CO, which acts as a poisoning species for the anode catalyst; methanol and ethanol, which have a relatively low reactivity at low temperatures) and the electro-reduction of the oxidant (oxygen), which is still a source of high energy losses (up to 30–40%) due to the low reactivity of oxygen at the best platinum-based electrocatalysts.

1.3

Low-temperature Fuel Cells (PEMFCs and DAFCs)

1.3.1

Proton Exchange Membrane Fuel Cell (PEMFC)

The PEMFC is nowadays the most advanced low-temperature fuel cell technology [19, 20], because it can be used in several applications (space programs, electric vehicles, stationary power plants, auxiliary power units, portable electronics). The progress made in one application is greatly beneficial to the others.

1.3.1.1 Principle of a PEMFC

An elementary PEMFC consists of a thin film (10–200 μm) of a solid polymer electrolyte (a protonic membrane, such as Nafion), on both sides of which the electrode structures (fuel anode and oxygen cathode) are pasted, giving a membrane–electrode assembly (MEA) (Figure 1.8). A single cell delivers a cell voltage of 0.5–0.9 V (instead of the theoretical emf of 1.23 V under standard equilibrium conditions), depending on the working current density. Many elementary cells, electrically connected by bipolar plates, are assembled together (in series and/or in parallel) to reach the nominal voltage (such as 48 V for electric vehicles) and the nominal power of the fuel cell stack.

In PEMFCs working at low temperatures (20–90 °C), several problems need to be solved before the technological development of fuel cell stacks for different applications. This concerns the properties of the components of the elementary cell, that is, the proton exchange membrane, the electrode (anode and cathode) catalysts, the membrane–electrode assemblies and the bipolar plates [19, 20]. This also concerns the overall system with its control and management equipment (circulation of reactants and water, heat exhaust, membrane humidification, etc.).

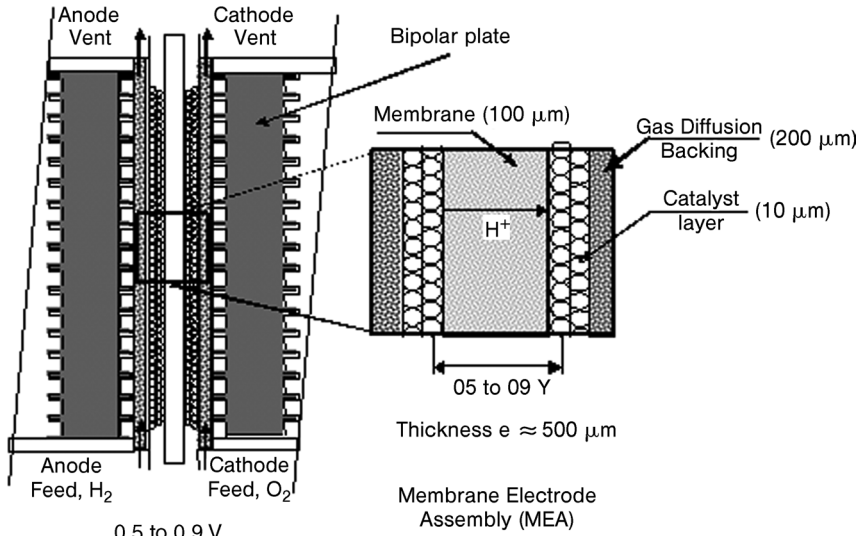


Figure 1.8 Schematic representation of a PEMFC elementary cell (and its MEA).

1.3.1.2 The Proton Exchange Membrane

The proton exchange membrane, which is a solid polymer electrolyte, plays a key role in the PEMFC. It allows the electrical current to pass through it thanks to its H⁺ ionic conductivity and prevents any electron current through it so that electrons are obliged to circulate in the external electric circuit to produce the electric energy corresponding to the combustion reaction of the fuel. Moreover, it must avoid any gas leakage between the anode and cathode compartments, so that no chemical combination between hydrogen and oxygen is directly allowed. It must also be mechanically, thermally (up to 150 °C in order to increase the working temperature of the cell) and chemically stable. Finally, its lifetime must be sufficient for practical applications (4 000 h for automotive to 40 000 h for stationary applications).

The actually developed PEMFCs have a Nafion membrane, which partially fulfills these requirements, since its thermal stability is limited to 100 °C and its proton conductivity decreases strongly at higher temperatures because of its dehydration. On the other hand, it is not completely tight to liquid fuels (such as alcohols). This becomes more important as the membrane is thin (a few tens of micrometers). Furthermore, its actual cost is too high (more than 500 € m⁻²), so that its use in a PEMFC for an electric car is not cost competitive.

Therefore, new membranes are being investigated with improved stability and conductivity at higher temperatures (up to 150 °C) [21]. For power FCs, the increase in temperature will increase the rate of the electrochemical reactions occurring at both electrodes, that is, the current density at a given cell voltage and the specific power. Furthermore, thermal management and heat utilization will be improved, particularly for residential applications with heat co-generation and for mobile applications to exhaust excess heat.

1.3.1.3 The Electrode Catalysts

One of the main problems with low-temperature (20–80 °C) PEMFCs is the relatively slow kinetics of the electrochemical reactions involved, such as oxygen reduction at the cathode and fuel (hydrogen from a reformat gas or alcohols) oxidation at the anode. The reaction rates can only be increased by the simultaneous action of the electrode potential and electrode material (electrocatalytic activation). Moreover, increasing the working temperature from 80 to 150 °C would strongly increase (by a factor of at least 100–1000) the rates of the electrochemical reactions (thermal activation). All these combined effects would increase the cell voltage by about 0.1–0.2 V, since at room temperature the anode and cathode overvoltages are close to 0.2–0.4 V, which decreases the cell voltage by 0.4–0.7 V, leading to values close to 0.5–0.7 V instead of the theoretical cell voltage of 1.23 V.

The investigation of new electrocatalysts, particularly Pt-based catalysts, that are more active for oxygen reduction and fuel oxidation (hydrogen from reformat gas or alcohols) is thus an important point for the development of PEMFCs [16, 17, 22, 23].

1.3.1.4 The Membrane–Electrode Assembly

The realization of the MEA is a crucial point for constructing a good fuel cell stack. The method currently used consists in hot-pressing (at 130 °C and 35 kg cm⁻²) the electrode structures on the polymer membrane (Nafion). This gives non-reproducible results (in terms of interface resistance) and this is difficult to industrialize. New concepts must be elaborated, such as the continuous assembly of the three elements in a rolling tape process (as in the magnetic tape industry) or successive deposition of the component layers (microelectronic process) and so on.

1.3.1.5 The Bipolar Plates

The bipolar plates, which separate both electrodes of neighboring cells (one anode of a cell and one cathode of the other), have a triple role:

- to ensure the electron conductivity between two neighboring cells;
- to allow the distribution of reactants (gases and liquids in the case of alcohols) to the electrode catalytic sites and to evacuate the reaction products (H₂O and CO₂ in the case of alcohols);
- thermal management inside the elementary cell by evacuating the excess heat.

The bipolar plates are usually fabricated with non-porous machined graphite or corrosion-resistant metal plates. Distribution channels are engraved in these plates. Metallic foams can also be used for distributing the reactants. One key point is to ensure a low ohmic resistance inside the bipolar plate and at the contact with the MEA. Another point is to use materials with high corrosion resistance in the oxidative environment of the oxygen cathode.

1.3.1.6 Auxiliary and Control Equipment

A more detailed picture of a PEMFC system, including the auxiliary and control equipments, is shown in Figure 1.9.

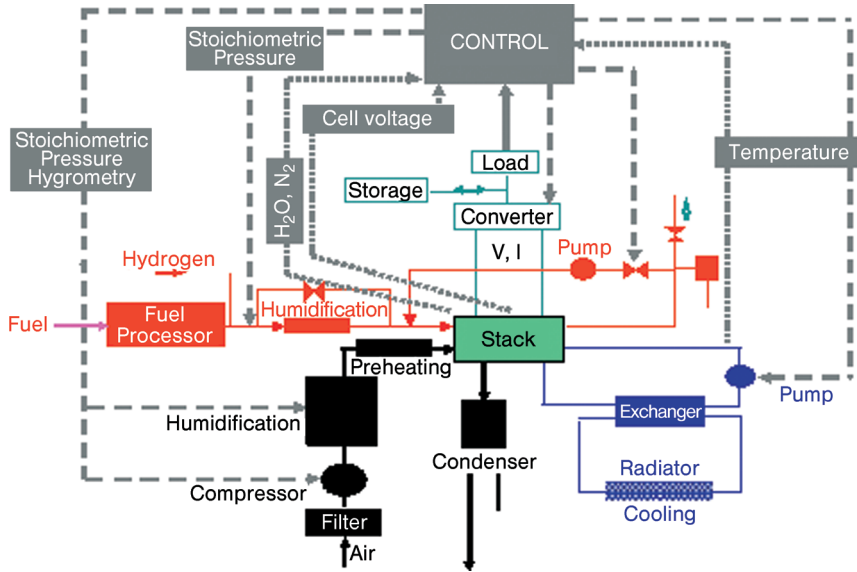


Figure 1.9 Detailed scheme of a PEMFC system with its auxiliary and control equipments.

Fuel supply is usually from liquid hydrogen or pressurized gaseous hydrogen. For other fuels, a fuel processor is needed, which includes a reformer, water gas shift reactors and purification reactors, in order to decrease the amount of CO to an acceptable level (below a few tens of ppm), which would otherwise poison the platinum-based catalysts. This equipment is still heavy and bulky and limits the dynamic response of the fuel cell stack, particularly for the electric vehicle in some urban driving cycles.

On the other hand, the other auxiliary equipment depends greatly on the stack characteristics:

- air compressor, the characteristics of which are related to the pressures supported by the proton exchange membrane;
- humidifiers for the reacting gases with controlled humidification conditions;
- preheating of gases to avoid condensation phenomena;
- hydrogen recirculation and purging systems of the anode compartment;
- cooling system for the MEAs;
- control of pressure valves and/or of gas flows;
- DC/DC or DC/AC electric converters.

The system control must ensure correct working of the system, not only under steady-state conditions, but also during power transients. All the elementary cells must be controlled (the cell voltage of each elementary cell, if possible) and the purging system must be activated in the case of a technical hitch.

According to different applications (stationary power plants, power sources for electric vehicle, auxiliary power units, etc.), different specifications and system design are required.

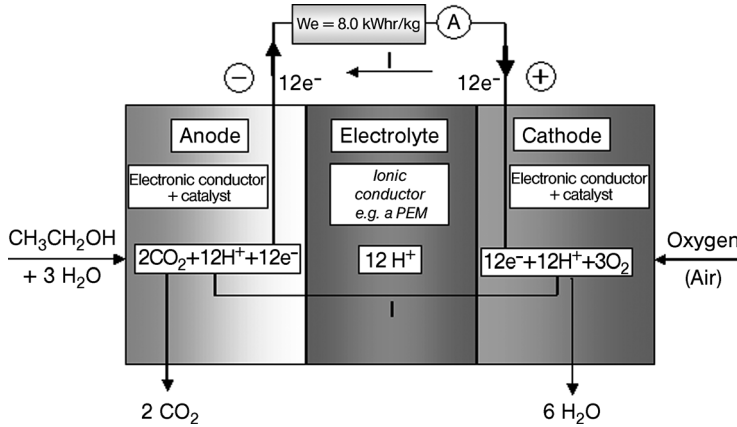


Figure 1.10 Schematic diagram of a DEFC.

1.3.2

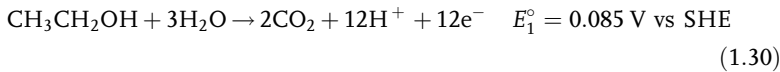
Direct Ethanol Fuel Cell (DEFC)

1.3.2.1 Principle of the Direct Ethanol Fuel Cell

A schematic diagram of a DEFC is shown in Figure 1.10.

The DEFC transforms directly the Gibbs energy of combustion of ethanol into electricity, without a fuel processor. This greatly simplifies the system, reducing its volume and cost [22, 23]. The important development of DEFCs is due to the use of a proton exchange membrane as electrolyte, instead of a liquid acid electrolyte, as done previously.

At the anode, the electro-oxidation of ethanol takes place as follows, leading, in the case of complete oxidation, to CO_2 :



whereas the electro-reduction of oxygen occurs at the cathode:



where E_i° are the electrode potentials versus SHE. This corresponds to the overall combustion reaction of ethanol into oxygen:



with the thermodynamic data, under standard conditions:

$$\Delta G^\circ = -1325 \text{ kJ mol}^{-1}; \Delta H^\circ = -1366 \text{ kJ mol}^{-1} \text{ of ethanol} \quad (1.33)$$

This gives a standard emf at equilibrium:

$$E_{\text{eq}}^\circ = -\frac{\Delta G^\circ}{nF} = \frac{1325 \times 10^3}{12 \times 96485} = E_2^\circ - E_1^\circ = 1.144 \text{ V} \quad (1.34)$$

with $n = 12$ the number of electrons exchanged per molecule for complete oxidation to CO_2 . The corresponding electrical energy, $W_{\text{el}} = nFE_{\text{eq}}^{\circ} = -\Delta G^{\circ}$, leads to a mass energy density $W_e = -\Delta G^{\circ}/(3600 M) = 8 \text{ kWh kg}^{-1}$, where $M = 0.046 \text{ kg}$ is the molecular weight of ethanol.

The theoretical energy efficiency, under reversible standard conditions, defined as the ratio between the electrical energy produced ($-\Delta G^{\circ}$) and the heat of combustion ($-\Delta H^{\circ}$) at constant pressure, is – see Equation 1.5

$$\epsilon_{\text{cell}}^{\text{rev}} = \frac{\Delta G^{\circ}}{\Delta H^{\circ}} = \frac{1325}{1366} = 0.97 \quad (1.35)$$

However, under working conditions, with a current density j , the cell voltage $E(j)$ is lower than E_{eq} – see Equation 1.7 – so that the practical energy efficiency, for a DEFC working at 0.5 V and 100 mA cm^{-2} with complete oxidation to CO_2 , would be – see Equation 1.9

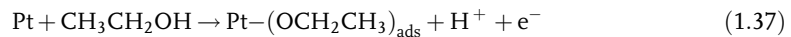
$$\epsilon_{\text{cell}}^{\text{C}_2\text{H}_5\text{OH/O}_2} = \epsilon_{\text{F}} \times \epsilon_{\text{E}} \times \epsilon_{\text{cell}}^{\text{rev}} = 1 \times 0.437 \times 0.97 = 0.424 \quad (1.36)$$

since the potential efficiency $\epsilon_{\text{E}} = E(j)/E_{\text{eq}} = 0.5/1.14 = 0.437$ and the faradaic efficiency $\epsilon_{\text{F}} = n_{\text{exp}}/n_{\text{th}} = 1$ for complete oxidation to CO_2 . This is similar to that of the best thermal engine (diesel engine). However, if the reaction process stops at the acetic acid stage, which involves the transfer of four electrons (instead of 12 for complete oxidation), the efficiency will be reduced by two-thirds, reaching only 0.15.

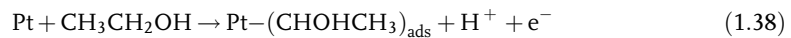
An additional problem arises from ethanol crossover through the proton exchange membrane. It results that the platinum cathode experiences a mixed potential, since both the oxygen reduction and ethanol oxidation take place at the same electrode. The cathode potential is therefore lower, leading to a decrease in the cell voltage and a further decrease in the voltage efficiency.

1.3.2.2 Reaction Mechanisms of Ethanol Oxidation

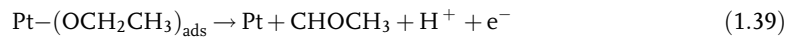
The electrochemical oxidation of ethanol has been extensively studied at platinum electrodes [22–34]. The first step is the dissociative adsorption of ethanol, either via an O-adsorption or a C-adsorption process [25, 26], to form acetaldehyde (AAL) according to the following reaction equations. Indeed, it was shown by Hitmi *et al.* [34] that AAL was formed at potentials lower than 0.6 V vs RHE. Thus:



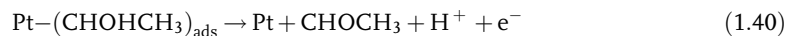
or



followed (at $E < 0.6 \text{ V}$ vs RHE) by

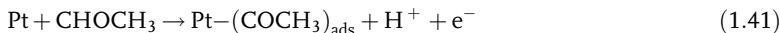


or

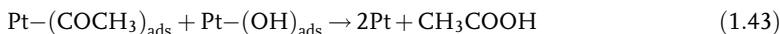


AAL has to be readsorbed to oxidize further either into acetic acid or carbon dioxide. To complete the oxidation reaction leading to both of these species, an extra oxygen atom is needed, which has to be brought by activated (adsorbed) water molecules at the platinum surface.

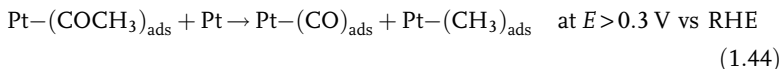
Thus, as soon as AAL is formed, it can adsorb on platinum sites leading to a Pt-COCH₃ species at $E < 0.6$ V vs RHE:



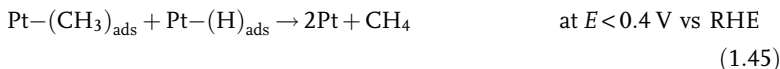
Further oxidation, without breaking of the -C-C- bond, may occur at potentials > 0.6 V vs RHE, through the activation of water molecules at platinum sites:



On the other hand, SNIFTIRS measurements have clearly shown that Pt is able to break the -C-C- bond, leading to adsorbed CO species at relatively low anode potentials (from 0.3 V vs RHE) [35]. However, Iwasita and Pastor [26] found some traces of CH₄ at potentials lower than 0.4 V vs RHE. Thus:



and



At potentials higher than 0.6 V vs RHE, the dissociative adsorption of water occurs on platinum, providing -OH adsorbed species, able to oxidize further the adsorption residues of ethanol. Then, oxidation of adsorbed CO species occurs as was shown by FTIR reflectance spectroscopy and CO stripping experiments [36]:



AAL can also be oxidized, leading to acetic acid (AA), as follows:



In a recent study, the analysis of the reaction products at the outlet of the anode compartment of a DEFC fitted with a Pt/C anode showed that only AA, AAL and CO₂ could be detected by HPLC [24]. Depending on the electrode potential, AAL, AA, CO₂ and traces of CH₄ are observed, the main products being AAL and AA (Table 1.2), AA being considered as a final product because it is not oxidized under smooth conditions. Long-term electrolysis experiments on a Pt catalyst show that AAL is detected at potentials as low as 0.35 V vs RHE, whereas no AA was detected in this potential range.

Table 1.2 Chemical yields in acetaldehyde, acetic acid and CO₂ for the electro-oxidation of ethanol at Pt/C, Pt–Sn (90:10)/C and Pt–Sn–Ru (86:10:4)/C catalysts under DEFC operating conditions at 80 °C for 4 h.

Parameter	Electrocatalyst		
	Pt/C	Pt _{0.9} Sn _{0.1} /C	Pt _{0.86} Sn _{0.1} Ru _{0.04} /C
Metal loading (wt%)	60	60	60
Current density(mA cm ⁻²)	8	32	32
Cell voltage(V)	0.3–0.35	0.45–0.49	0.5–0.55
AAI/Σ products (%)	47.5	15.4	15.2
AA/Σ products (%)	32.5	76.9	75
CO ₂ /Σ products (%)	20	7.7	9.8

From the results given in Table 1.2, it appears that the addition of tin to platinum greatly favors the formation of AA compared with AAL, as explained by the bifunctional mechanism [14].

Several added metals were investigated to improve the kinetics of ethanol oxidation at platinum-based electrodes, including ruthenium [27, 28], lead [29] and tin [22, 30]. Of these, tin appeared to be very promising. Figure 1.11 shows the polarization curves of ethanol electro-oxidation recorded at a slow sweep rate (5 mV s⁻¹) on different platinum-based electrodes. Pt–Sn(0.9:0.1)/C displays the

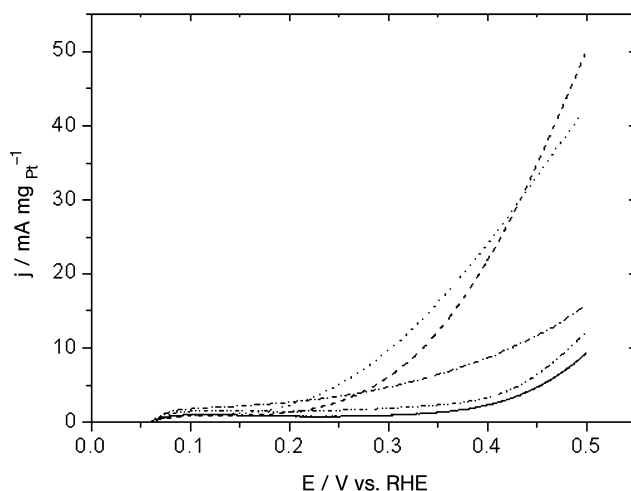
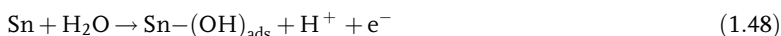


Figure 1.11 Electro-oxidation of ethanol on Pt/C (full line) and different Pt-based (dashed and dotted lines) catalysts with 0.1 mg Pt cm⁻² loading. 0.1 M HClO₄ + 1 M C₂H₅OH; 5 mV s⁻¹; 3000 rpm; 20 °C. (—), Pt/XC72; (-----), Pt–Sn (90:10)/XC72; (·····), Pt–Sn (80:20)/XC72; (-·-·-·-), Pt–Ru (80:20)/XC72; (-·-·-·-), Pt–Mo (80:20)/XC72.

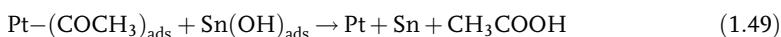
best activity in the potential range 0.15–0.5 V vs RHE, as it gives a higher oxidation current density than the other catalysts. The role of tin can also be established by analyzing the distribution of reaction products at the anode outlet of a fuel cell fitted with a Pt–Sn(0.9:0.1)/C anode and from *in situ* IR reflectance spectroscopic measurements [24, 37].

Table 1.2 indicates that alloying platinum with tin led to important changes in the product distribution: an increase in the AA chemical yield and a decrease in the AAL and CO₂ chemical yields. The presence of tin seems to allow, at lower potentials, the activation of water molecules and the oxidation of AAL species into AA. In the same manner, the amount of CO₂ decreased, which can be explained by the need for several adjacent platinum atoms (three or four) to realize the dissociative adsorption of ethanol into CO species, via breaking the C–C bond. In the presence of tin, ‘dilution’ of platinum atoms can limit this reaction. The effect of tin, in addition to the activation of water molecules, may be related to some electronic effects (ligand effects) on the CO oxidation reaction [38].

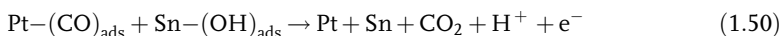
On Pt–Sn, assuming that ethanol adsorbs only on platinum sites, the first step can be the same as for platinum alone. However, as was shown by SNIFTIRS experiments [37], the dissociative adsorption of ethanol on a PtSn catalyst to form adsorbed CO species takes place at lower potentials than on a Pt catalyst, between 0.1 and 0.3 V vs RHE, whereas on a Pt catalyst the dissociative adsorption of ethanol takes place at potentials between 0.3 and 0.4 V vs RHE. Hence it can be stated that the same reactions occur at lower potentials and with relatively rapid kinetics. Once intermediate species such as Pt–(COCH₃)_{ads} and Pt–(CO)_{ads} are formed, they can be oxidized at potentials close to 0.3 V vs RHE, as confirmed by CO stripping experiments, because OH species are formed on tin at lower potentials [39, 40]:



then adsorbed acetyl species can react with adsorbed OH species to produce AA according to



Similarly, Pt–(CO)_{ads} species are oxidized as follows:



This mechanism explains also the higher efficiency of Pt–Sn in forming AA compared with Pt at low potentials ($E < 0.35$ V vs RHE), as was shown by electrolysis experiments. Indeed, adsorbed OH species on Sn atoms can be used to oxidize adsorbed CO species to CO₂ or to oxidize adsorbed –COCH₃ species to CH₃COOH, according to the bifunctional mechanism [14].

On the other hand, the yield of CO₂ with a Pt/C catalyst is double that with a Pt–Sn/C catalyst (see Table 1.2). This can be explained by the need to have several adjacent platinum sites to adsorb dissociatively the ethanol molecule and to break the C–C bond. As soon as some tin atoms are introduced between platinum atoms, this latter reaction is disadvantaged.

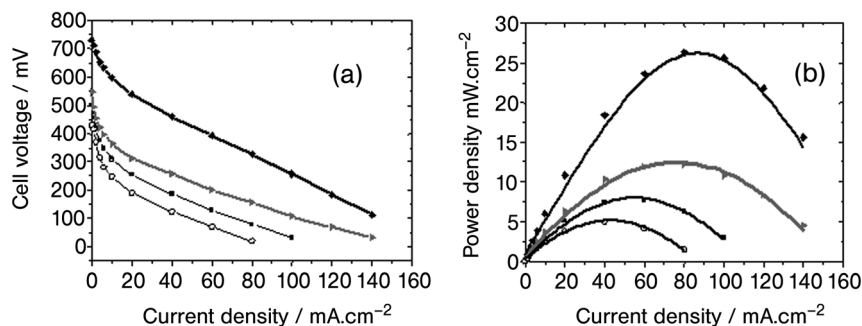


Figure 1.13 Fuel cell characteristics of a 5 cm² DEFC recorded at 110 °C. Influence of the nature of the bimetallic catalysts (80:20 atomic ratio with 30% metal loading). Anode catalyst, 1.5 mg cm⁻²; cathode catalyst, 2 mg cm⁻² (40% Pt/XC72 from E-TEK); membrane, Nafion 117; ethanol concentration, 1 M. (■) Pt/XC72; (◆) Pt-Sn (80:20)/XC72; (▲) Pt-Ru (80:20)/XC72; (◇) Pt-Mo (80:20)/XC72.

The experiments were carried out using Pt/C, Pt-Sn/C and Pt-Sn-Ru/C catalysts and in each case no other reaction products than AAL, AA and CO₂ were detected. The addition of tin to platinum not only increases the activity of the catalyst towards the oxidation of ethanol and therefore the electrical performance of the DEFC, but also changes greatly the product distribution: the formation of CO₂ and AAL is lowered, whereas that of AA is greatly increased (Table 1.2).

Typical electrical performances obtained with several Pt-based electrocatalysts are shown in Figure 1.13. The use of platinum alone as anode catalyst leads to poor electrical performance, the open circuit voltage (OCV) being lower than 0.5 V and the maximum current density reaches only 100 mA cm⁻², leading to a maximum power density lower than 7 mW cm⁻² at 110 °C. The addition of Ru and especially of Sn to platinum in the anode catalyst greatly enhances the electrical performance of the DEFC by increasing the OCV to 0.75 V, which indicates that the modified catalysts are less poisoned by adsorbed species coming from ethanol chemisorption than the Pt/C catalyst. For Pt-Sn (80:20), current densities up to 150 mA cm⁻² are reached at 110 °C, giving a maximum power density greater than 25 mW cm⁻², which means an electrical performances four times higher than those obtained with Pt/C. The increase in the electrical performance indicates that the bimetallic catalyst is more active for ethanol electro-oxidation than the Pt/C catalyst.

With the best electrocatalyst, that is, Pt-Sn (90:10)/XC72, the effect of temperature on the cell voltage E and power density P versus current density j characteristics is shown in Figure 1.14. It appears clearly that increasing the temperature greatly increases the performance of the cell, from a maximum power density close to 5 mW cm⁻² at 50 °C to 25 mW cm⁻² at 110 °C, that is, five times higher.

This confirms the difficulty of oxidizing ethanol at low temperatures and the necessity to work at temperatures higher than 100 °C to enhance the electrode kinetics and, thus, the performance of the DEFC.

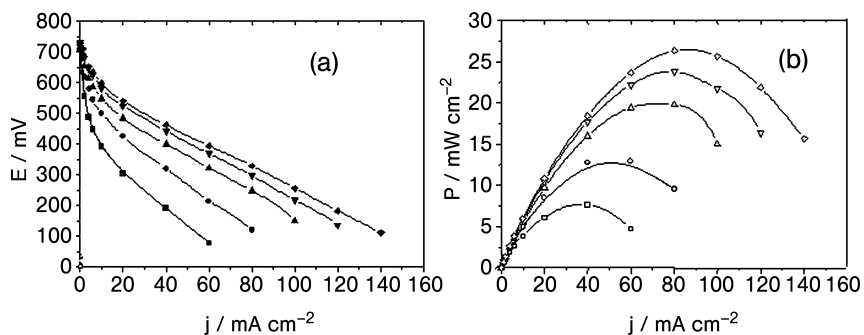


Figure 1.14 Fuel cell characteristics of a 25 cm² DEFC recorded with a 30% Pt–Sn (90 : 10) catalyst. Influence of the working temperature. Anode catalyst, 1.5 mg cm⁻² [30% Pt–Sn (90 : 10)/XC72]; cathode catalyst, 2 mg cm⁻² (40% Pt/XC72 from E-TEK); membrane, Nafion 117; ethanol concentration, 1 M. (■) 50 °C; (●) 70 °C; (▲) 90 °C; (▼) 100 °C; (◆) 110 °C.

Finally the performance of a DEFC with an anode containing a higher amount of platinum (i.e. 60 wt% instead of 30 wt% for the previous experiments) were determined with three Nafion membranes, N117, N115 and N112, of different thickness (180, 125 and 50 μm, respectively) to investigate the effect of ethanol crossover through the membrane. Figure 1.15 shows the ethanol crossover as measured by following the ethanol concentration in a second cell compartment, initially containing no ethanol, separated by the Nafion membrane from the first one containing 1 M ethanol. The crossover rate through N117 is about half that through N112. The better behavior of N117 is confirmed in Figure 1.16, showing the comparative electrical characteristics of a DEFC having as electrolyte one of the three Nafion membranes and an anode with a higher platinum loading (60% Pt–Sn (90 : 10)/XC72): the DEFC with N117 displays the highest OCV (0.8 V) and leads to a power density of 52 mW cm⁻² at 90 °C.

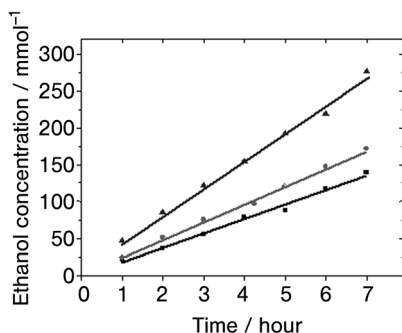


Figure 1.15 Behavior of different Nafion membranes. Ethanol permeability measurements of different Nafion membranes. T = 25 °C. (■) Nafion 117; (●) Nafion 115; (▲) Nafion 112.

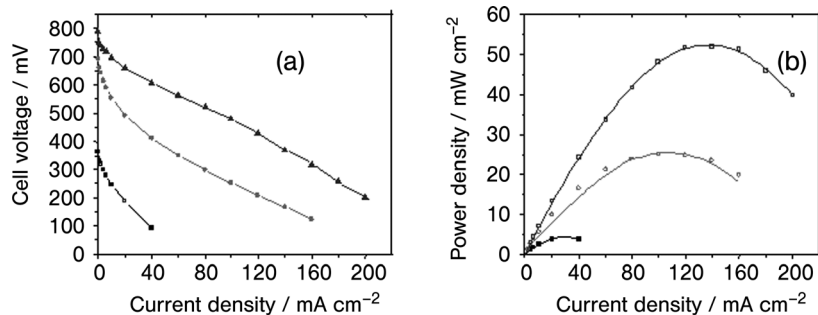


Figure 1.16 Fuel cell characteristics of a DEFC recorded at 90 °C with a 60% Pt–Sn (90 : 10)/XC72 catalyst for different Nafion membranes. (▲) Nafion 117; (●) Nafion 115; (■) Nafion 112.

1.4

Solid Alkaline Membrane Fuel Cell (SAMFC)

The rate of oxidation of alcohols [41] and reduction of oxygen [41, 42] is higher in alkaline than acidic media, so that the use of an AEM instead of a PEM brings new opportunities to develop DEFC with the concept of a SAMFC. For that purpose, in addition to the choice of an AEM with sufficiently good conductivity and stability, the investigation of electrode reaction catalysts, particularly non-noble metals, is challenging.

1.4.1

Development of a Solid Alkaline Membrane for Fuel Cell Application

The first key component of a membrane fuel cell is the membrane electrolyte. Its central role lies in the separation of the two electrodes and the transport of ionic species (e.g. hydroxyl ion, OH⁻, in an AEM), between them. In general, quaternary ammonium groups are used as anion-exchange groups in these materials. However, due to their low stability in highly alkaline media [43, 44], only a few membranes have been evaluated for use as solid polymer electrolytes in alkaline fuel cells.

The first methanol-fed PEMFC working with an AEM was conceived by Hunger in 1960 [15, 45]. This system contained an AEM with porous catalytic electrodes pressed on both sides and led to relatively poor electrical performance (1 mA cm⁻² at 0.25 V at room temperature with methanol and air as the reactants). Since this first attempt, many studies have been carried out to develop alkaline membranes.

Chloromethylated aromatic polymers of the polycondensation type are generally used to produce strongly alkaline AEMs [46]. The backbone positive charge of AEMs is generally provided by quaternary ammonium groups. For instance, Fang and Shen developed a quaternized poly(phthalazinone ether sulfone ketone) membrane (PESK) for alkaline fuel cell applications [47]. They obtained a maximum conductivity ranging from 5.2×10^{-3} to 0.14 S cm^{-1} depending on the concentration of the KOH solution and good thermal stability of the polymer up to 150 °C. Quaternized

polyether sulfone cardo polymers (QPES-C) were also studied by Li *et al.* [48, 49]. They determined their conductivity and permeability to methanol. The conductivity of the membrane in 1.0 M NaOH solution increased from 4.1×10^{-2} to 9.2×10^{-2} S cm⁻¹ with increase in temperature from room temperature to 70 °C, whereas the methanol diffusion coefficient inside the membrane increased from 5.7×10^{-8} to 1.2×10^{-7} cm² s⁻¹ over this temperature range, which is at least 40 times lower than those for a Nafion membrane [49]. Although these membranes display high ionic conductivity, high thermal stability and low methanol permeability and therefore they may be suitable for use in direct alcohol alkaline fuel cells, no fuel cell data are available so far to compare with the current performance of DEFCs.

Another important class of membranes studied for SAMFC application is prepared from perfluorinated backbone polymers. Yu and Scott studied the electrochemical performance of an alkaline DMFC working with an AEM [50]. The commercial ADP-Morgane membrane provided by Solvay consisted of a cross-linked fluorinated polymer carrying quaternary ammonium as exchange groups. Its thickness in the fully humidified state is 150–160 μm and its specific resistance in 1 M NaOH solution is close to 0.5 Ω cm². The fuel cell performance gave a maximum power density close to 10 mW cm⁻² with a Pt/C anode (60 wt% Pt, 2.19 mg cm⁻² on non-Teflonized Toray 90 carbon paper) and a Pt/C cathode (60 wt% Pt, 2.07 mg cm⁻² on 20% wet-proofed Toray 90 carbon paper), at a cell operating temperature of 60 °C and air pressure of 2 bar in 2 M methanol and 1 M NaOH. This membrane was also used by Demarconnay and co-workers to compare the performance of a direct methanol fuel cell with that of a direct ethylene glycol fuel cell [51, 52]. In both cases, they obtained a maximum power density close to 20 mW cm⁻² at 20 °C, with similar electrodes mechanically pressed against the membrane (Pt 40 wt%/C, 2.0 mg Pt cm⁻²), using pure oxygen at a pressure of 1 bar and 2 M methanol in 1 M NaOH. Varcoe and co-workers developed and characterized quaternary ammonium radiation grafted alkaline anion-exchange membranes (AAEMs), such as poly(ethylene-co-tetrafluoroethylene) (ETFE) [53, 54] and poly(hexafluoropropylene-co-tetrafluoroethylene) (FEP) with ion-exchange capacity as high as 1.35 meq OH⁻ g⁻¹ and conductivity (as determined from electrochemical impedance spectroscopy) up to 0.023 ± 0.001 S cm⁻¹ at 50 °C, which are between 20 and 50% of the values for the commercial acid-form Nafion115 membrane [55, 56]. In order to avoid carbonation of the electrode (carbonate precipitation) and to improve the long-term operation stability, they worked in fuel solutions without the undesirable addition of M⁺ OH⁻. A peak power density of 130 mW cm⁻² for an H₂/O₂ fuel cell was obtained, while a maximum power density of 8.5 mW cm⁻² was obtained in a metal cation-free methanol/O₂ fuel cell working at 2–2.5 bar back-pressure and 80 °C.

However, fluorine-containing polymers are expensive and the use of hydrocarbon-only membranes (C–H backbone) could be interesting considering their manufacturing and availability. According to Hübner and Roduner [57], at high *in situ* pH, the oxidative radical mechanism for polymer degradation is suppressed. Moreover according to Matsuoka *et al.* [58], an alcohol penetrating the AEM may protect it from attack by peroxide. They used a polyolefin backbone chain from Tokuyama (Japan), on which was fixed tetraalkylammonium groups giving a membrane with

a thickness of 240 μm . The conductivity of this membrane was close to 14 mS cm^{-1} . Alkaline direct alcohol fuel cell tests were performed with 1.0 M of different alcohols (methanol, ethylene glycol, *meso*-erythritol, xylitol) in 1.0 M KOH, with a $1.0 \text{ mg Pt cm}^{-2}$ Pt/C catalyst as cathode and $4.5 \text{ mg Pt-Ru cm}^{-2}$ Pt-Ru/C catalyst as anode. Ethylene glycol led to the highest power density (9.8 mW cm^{-2}) at 50°C .

Agel *et al.* [59] and Stoica *et al.* [60] also used non-fluorine-containing polymers, such as polyepichlorhydrin homo- and copolymers. The ionic conduction of these polymers, which can be assimilated to polyether polymers, is insured by the presence of quaternary ammonium groups as exchange groups. An ion-exchange capacity of 1.3 mol kg^{-1} and a conductivity of $1.3 \times 10^{-2} \text{ S cm}^{-1}$ at 60°C and $\text{RH} = 98\%$ were found with ionomers based on polyepichlorhydrin copolymers using allyl glycidyl ether as cross-linking agent, but no fuel cell results were given. However, using a polyepichlorhydrin homopolymer, H_2/O_2 fuel tests were carried out without and with an interfacial solution made of poly(acrylic acid) and 1 M KOH between the electrodes and the membrane, giving maximum power densities close to 20 and 40 mW cm^{-2} , respectively, at 25°C with $P_{\text{O}_2} = P_{\text{H}_2} = 1 \text{ bar}$ and electrodes containing $0.13 \text{ mg Pt cm}^{-2}$.

The plasma route for the synthesis of conductive polymers was developed recently [61]. Starting from a monomer containing triethylamine or triallylamine groups, the membrane is synthesized by plasma polymerization of the monomer vapor in a glow discharge to form a thin film partially composed of amine functions. Then, the amine functions are quaternized through methylation by immersion of the plasma film in methyl iodide solution. The structure of the plasma membranes consists of a polyethylene-type matrix containing a mixture of primary, secondary, tertiary and quaternary amine groups. The polymers are amorphous, dense materials, highly cross-linked, and show a disorganized structure. Electrochemical impedance spectroscopic measurements revealed a rather low ion-exchange capacity and low conductivity, but this could be counterbalanced by their low thickness (a few microns).

All the membranes considered were based on quaternary ammonium groups as anion-exchange groups. However, these conductive groups may decompose in concentrated alkaline solution following the Hofmann degradation reaction [43]. It is crucial how these groups are attached to the polymer backbone, especially if one considers that, during fuel cell operation, the pH may increase up to 14. Under these conditions, the presence of β -hydrogen atoms with respect to the nitrogen atom may represent a serious drawback for the stability in alkaline media [62]. The decomposition of the backbone polymer matrix represents another factor to be taken into account when designing an effective AEM. Basically, so far there does not exist any stable AEM in concentrated sodium hydroxide solution at high temperature. Although perfluorinated cation-exchange membranes show excellent stability in the presence of oxidizing agents and concentrated hydroxide solution, a stable perfluorinated amine is difficult to obtain because of the specific properties of fluorine compounds, which readily decompose as follows:



Thus, some workers have investigated a completely different approach by using polymer films and introducing OH^- conductivity by treating the films with concentrated KOH. For example, poly(vinyl alcohol) (PVA) cross-linked with sulfosuccinic acid [63] or glutaraldehyde [64], doped with TiO_2 and so on, [64], were developed by Yang *et al.* The DMFC, consisting of an MnO_2/C air cathode, a Pt–Ru black/C anode and a PVA/ TiO_2 composite polymer membrane, allowed a maximum peak power density of about 7.5 mW cm^{-2} to be reached at 60°C and 1 bar in $2 \text{ M KOH} + 2 \text{ M CH}_3\text{OH}$ solution. Xing and Savadogo [65] developed a $40 \mu\text{m}$ thick alkali-doped polybenzimidazole (PBI) membrane, which exhibited ionic conductivity as high as $9 \times 10^{-2} \text{ S cm}^{-1}$ with 6 M KOH -doped PBI at 90°C . The performance of an H_2/O_2 SAMFC based on the KOH-doped PBI was similar to that of an H_2/O_2 PEMFC with Nafion 117, that is, close to $0.7\text{--}0.8 \text{ W cm}^{-2}$.

1.4.2

Anodic Catalysts in Alkaline Medium

Platinum-based catalysts are widely used in low-temperature fuel cells, so that up to 40% of the elementary fuel cell cost may come from platinum, making fuel cells expensive. The most electroreactive fuel is, of course, hydrogen, as in an acidic medium. Nickel-based compounds were used as catalysts in order to replace platinum for the electrochemical oxidation of hydrogen [66, 67]. Raney Ni catalysts appeared among the most active non-noble metals for the anode reaction in gas diffusion electrodes. However, the catalytic activity and stability of Raney Ni alone as a base metal for this reaction are limited. Indeed, Kiros and Schwartz [67] carried out durability tests with Ni and Pt–Pd gas diffusion electrodes in 6 M KOH medium and showed increased stability for the Pt–Pd-based catalysts compared with Raney Ni at a constant load of 100 mA cm^{-2} and at temperatures close to 60°C . Moreover, higher activity and stability could be achieved by doping Ni–Al alloys with a few percent of transition metals, such as Ti, Cr, Fe and Mo [68–70].

In the case of an SAMFC, working with a Pt/C anode and fuelled with either methanol or ethylene glycol, very similar power densities are achieved, that is, both are close to 20 mW cm^{-2} at 20°C , as shown in Figure 1.17 [51].

However, the most extensively investigated anode catalysts for DEFCs, in either acidic or alkaline media, contain binary and ternary combinations based almost exclusively on Pt–Ru and Pt–Sn [71, 72]. The superior performance of these binary and ternary electrocatalysts for the oxidation of ethanol, compared with Pt alone, is attributed to the bifunctional mechanism [14] and to the electronic interaction between Pt and the alloying metals [73]. Matsuoka *et al.* [74] studied the electro-oxidation of different alcohols and polyols for direct alkaline fuel cell applications using an AEM (from Tokumaya, Japan) functionalized with tetraalkylammonium groups as cationic groups (thickness = $240 \mu\text{m}$). They obtained the best performance with ethylene glycol, achieving a maximum power density close to 10 mW cm^{-2} with a Pt–Ru catalyst at the anode. The relatively good reactivity of ethylene glycol (EG) makes it a good candidate for SAMFC applications. It is less toxic than methanol, its specific energy is close to that of alcohols and both carbons carry alcoholic groups. It can then be

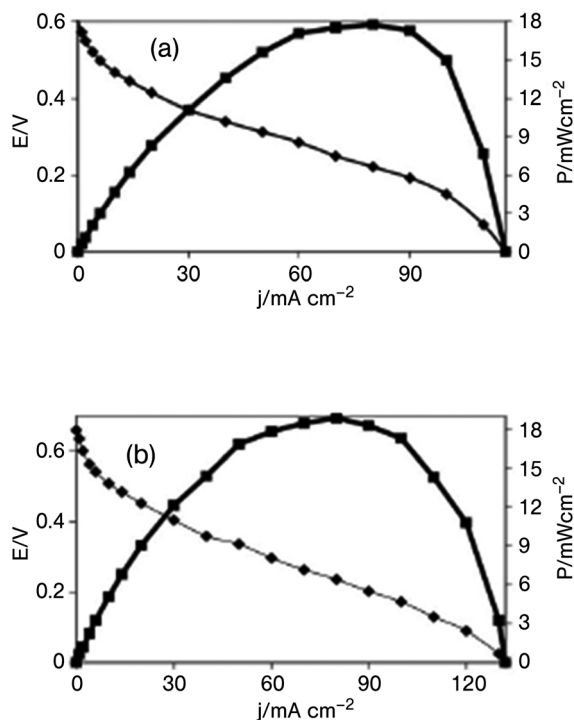


Figure 1.17 Cell voltage and power density vs current density curves for (a) 2 M methanol in 4 M NaOH solution; (b) 2 M ethylene glycol in 4 M NaOH solution. Anode and cathode catalysts, laboratory-made Pt (40 wt%)/C prepared via the Bönemann method, 2 mg Pt cm⁻²; commercial anionic membrane, Morgane ADP from Solvay; $T = 20^\circ\text{C}$.

assumed that its oxidation into oxalate species ($^-\text{COO}-\text{COO}^-$) can be achieved, as proposed by several authors [75–79]. Thus, 8 mol of electrons are exchanged per mole of EG, instead of 10 for complete oxidation into CO_2 , which means a faradaic efficiency of 80%. Metals other than Pt, such as Pd [80, 81], Au [82], Sn, Cd and Pb [83], display or enhance the catalytic activity towards EG electro-oxidation. Kadirgan *et al.* studied the effect of bismuth adatoms deposited on platinum surface by underpotential deposition (UPD) [84, 85]. They observed that the activity towards EG electro-oxidation is decreased in acidic medium, whereas it is highly enhanced in alkaline medium. Cnobloch *et al.* used catalysts containing Pt–PdBi as anode for an AFC working with 6 M KOH electrolyte [86]. A power of 225 W with a 52-cell stack was achieved. Coutanceau *et al.* studied the electrocatalytic behavior of nanostructured $\text{Pt}_{1-x}\text{Pd}_x/\text{C}$ towards EG electro-oxidation [51]. The highest electroactivity was found with a Pt:Pd atomic ratio of ca 1 : 1 for a metal loading on carbon of 20%, as shown in Figure 1.18. The synergetic effect of palladium when added to platinum was confirmed in an SAMFC by comparing the cell performance obtained at 20°C using a Pt (20 wt%)/C anode with that obtained using a $\text{Pt}_{0.5}\text{Pd}_{0.5}$ (20 wt%)/C anode (Figure 1.19).

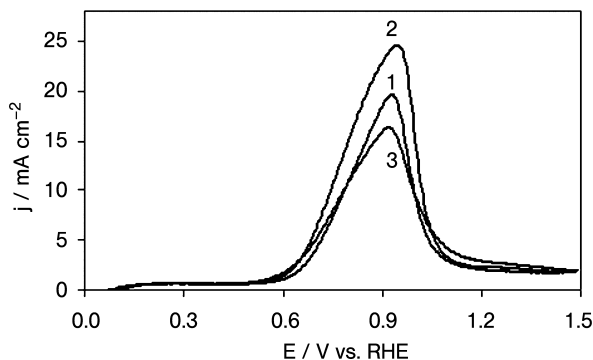


Figure 1.18 Polarization curves for the oxidation of 0.1 M ethylene glycol in 0.2 M NaOH solution recorded on (1) Pt_{0.25}Pd_{0.75} (20 wt%)/C, (2) Pt_{0.5}Pd_{0.5} (20 wt%)/C and (3) Pt_{0.75}Pd_{0.25} (20 wt%)/C; $\nu = 50 \text{ mV s}^{-1}$; $T = 20^\circ \text{C}$. Catalysts were prepared according to the Bönemann method.

Pt_{1-x}Bi_x/C and Pt_{1-(x+y)}Pd_xBi_y/C catalysts were also studied for EG electro-oxidation in alkaline medium [52]. The highest electrocatalytic activity was found for the atomic compositions Pt_{0.9}Bi_{0.1} and Pt_{0.45}Pd_{0.45}Bi_{0.1}. On the basis of electrochemical, *in situ* IR reflectance spectroscopy and high-performance liquid chromatography (HPLC) measurements, it was shown that the modification of platinum and platinum-palladium catalysts with bismuth led to the decrease in the CO₂ and formic acid yields (e.g. in the ability to break the C–C bond), whereas the yield in oxalic acid was increased, as shown in Figure 1.20a and b in the case of Pt/C and Pt_{0.45}Pd_{0.45}Bi_{0.1}, respectively. The different Bi-containing catalysts were used in a 5 cm² SAMFC anode and compared with respect to the electro-oxidation of EG (Figure 1.21). Finally, the activity increases in the following order: Pd/C < Pt/C < Pt–Pd/C < Pt–Bi < C < Pt–Pd–Bi/C.

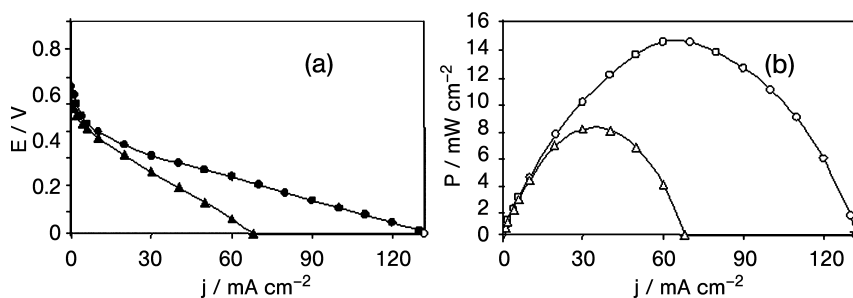


Figure 1.19 (a) Cell voltage and (b) power density vs current density curves recorded at 20 °C for the oxidation of 2 M ethylene glycol in 4 M NaOH. Anodes: (▲, △) Pt (20 wt%)/C and (●, ○) Pt_{0.5}Pd_{0.5} (20 wt%)/C. Laboratory-made cathode Pt (40 wt%)/C and anode catalysts prepared according to the Bönemann method. All electrodes were loaded with 2 mg cm⁻² of metal. Anionic membrane, Morgane ADP from Solvay.

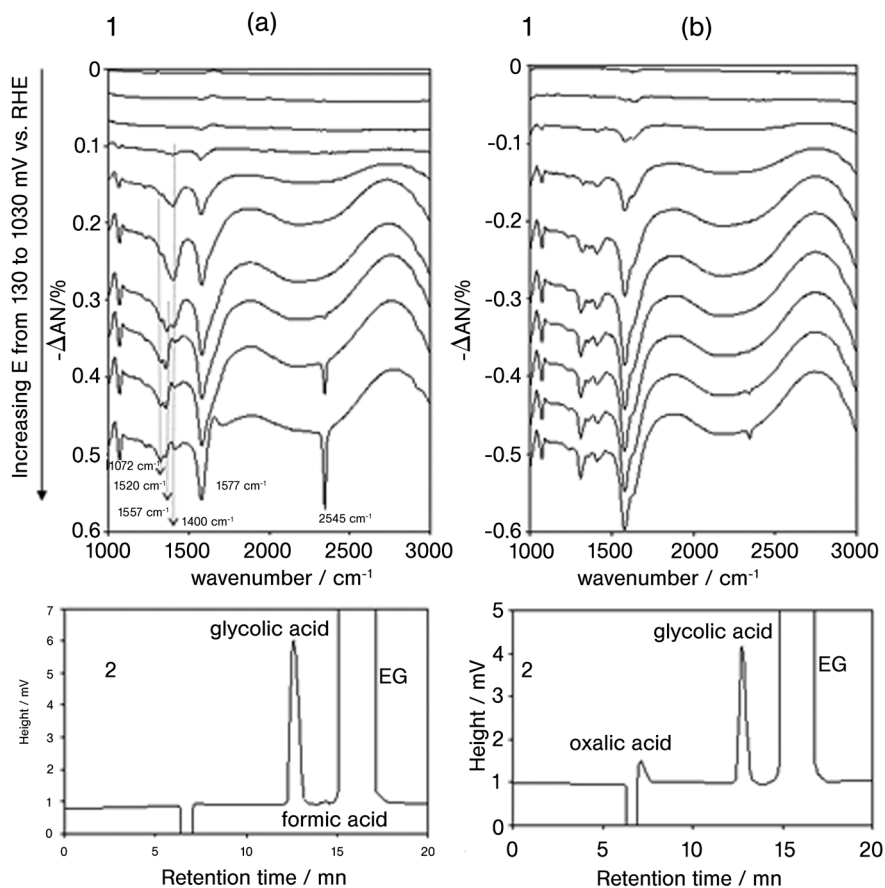


Figure 1.20 (a) SPAIR spectra recorded during the electro-oxidation of ethylene glycol on Pt/C in 0.2 M NaOH + 0.1 M EG, at various potentials (each 100 mV) from 130 to 1030 mV/RHE (1) and chromatograms of the anodic outlet of a SAMFC working with a Pt/C anode without fuel recirculation (2). Electro-catalysts were prepared according to the ‘water-in-oil’ microemulsion method. (b) SPAIR spectra recorded during the electro-oxidation of ethylene glycol on $\text{Pt}_{0.45}\text{Pd}_{0.45}\text{Bi}_{0.1}/\text{C}$ in 0.2 M NaOH + 0.1 M EG, at various potentials (each 100 mV) from 130 to 1030 mV/RHE (1) and chromatograms of the anodic outlet of a SAMFC working with a $\text{Pt}_{0.45}\text{Pd}_{0.45}\text{Bi}_{0.1}/\text{C}$ anode without fuel recirculation (2). Electro-catalysts were prepared according to the ‘water-in-oil’ microemulsion method.

In the case of ethanol, Pd-based electrocatalysts seem to be slightly superior to Pt-based catalysts for electro-oxidation in alkaline medium [87], whereas methanol oxidation is less activated. Shen and Xu studied the activity of Pd/C promoted with nanocrystalline oxide electrocatalysts (CeO_2 , Co_3O_4 , Mn_3O_4 and nickel oxides) in the electro-oxidation of methanol, ethanol, glycerol and EG in alkaline media [88]. They found that such electrocatalysts were superior to Pt-based electrocatalysts in terms of activity and poison tolerance, particularly a Pd–NiO/C electrocatalyst, which led to a negative shift of the onset potential of the oxidation of ethanol by ca 300 mV compared

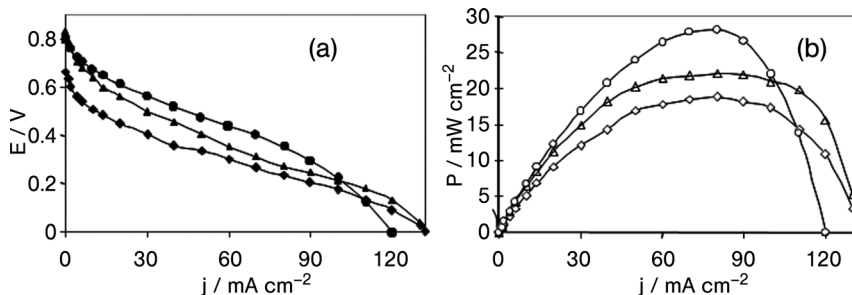


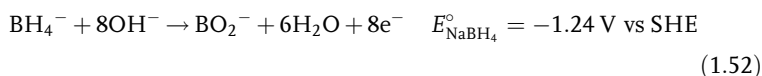
Figure 1.21 (a) Cell voltage and (b) power density vs current density curves recorded at 20 °C for the oxidation of 2 M ethylene glycol in 4 M NaOH. Anodes: (◆, ◇) Pt (40 wt%)/C; (▲, △) Pt_{0.9}Bi_{0.1} (50 wt%)/C; (●, ○) Pt_{0.45}Pd_{0.45}Bi_{0.1} (50 wt%)/C. Laboratory-made

cathode catalyst Pt (40 wt%)/C prepared according to the Bönemann method. Anode catalysts prepared according to the 'water-in-oil' microemulsion method. All electrodes were loaded with 2 mg cm⁻² of metal. Anionic membrane was Morgane-ADP from Solvay.

with a Pt/C electrocatalyst under the same experimental conditions. Recently, nanostructured electrocatalysts based on Fe–Co–Ni alloys, known with the acronym HYPERMEC [89], were synthesized. Electrodes containing these catalysts have proved to be efficient in DEFCs with anion-exchange membranes, delivering power densities as high as 30–40 mW cm⁻² at room temperature in self-breathing cells and up to 60 mW cm⁻² at 80 °C in active systems. However, the catalyst durability is relatively low due to the slow formation of a metal oxide layer on the metal particle surface [90]. But preliminary data from CNR and ACTA show unequivocally that the catalyst stability with time under working conditions can be remarkably improved, up to several thousand hours, by decorating non-noble metal catalysts with tiny amounts of palladium using original electroless or spontaneous deposition techniques [91].

However, the oxidation reaction of alcohol is very difficult to activate at low temperature, even in alkaline medium. This leads to poor cell performance. Other hydrogen 'reservoirs' were then studied for fuelling the SAMFC. Among them, NaBH₄ seems to be the most promising one [in that case the direct fuel cell is called the direct borohydride fuel cell (DBFC)]. Indeed, the specific energy density of NaBH₄ is about 9.3 kW h kg⁻¹ [92, 93], that is, higher than that of ethanol (8.0 kW h kg⁻¹). However, several oxidation paths are possible:

- the direct oxidation path:



- the indirect oxidation path:



Assuming an electrode potential of 0.40 V vs SHE for oxygen reduction in a 1 M alkaline medium ($\text{pH} = 14$), the direct path gives a cell voltage of 1.64 V, whereas the indirect path leads to a cell voltage of 1.23 V. Therefore, catalysts which favor the direct oxidation path are preferable in order to achieve higher cell performance and higher energy efficiency. First, this implies working in alkaline solution with pH higher than 12 in order to limit the borohydride hydrolysis reaction [94]. According to Elder and Hickling [95], only Pt, Pd and Ni, which display good activity for ionizing hydrogen, are able to oxidize borohydride at low overvoltages. Liu and co-workers [96, 97] achieved a power density of 35 mW cm^{-2} at room temperature with a DBFC working with a nickel-based anode and a silver-based cathode and of 290 mW cm^{-2} at 60°C with a mixture of surface-treated Zr–Ni Laves phase alloys, AB_2 ($\text{Zr}_{0.9}\text{Ti}_{0.1}\text{Mn}_{0.6}\text{V}_{0.2}\text{Co}_{0.1}\text{Ni}_{1.1}$), and Pd deposited on carbon as anode catalyst and platinum as cathode catalyst. However, these catalysts also activate greatly the hydrolysis reaction of borohydride and therefore favor the indirect oxidation path. Gold is known to be an active metal for the electro-oxidation of borohydride and inactive for that of hydrogen. According to Chatenet *et al.* [98], gold allows an almost complete utilization of the reducer since around 7.5 electrons per borohydride molecule are consumed with this material versus 4 with platinum. However, the onset potential of BH_4^- oxidation is shifted from about 0 V vs RHE with a Pt/C catalyst to about 0.35 V vs RHE with a Au/C catalyst, as shown in Figure 1.22.

Subsequently, to obtain a powerful DBFC system with high efficiency, Latour and co-workers proposed to manage the hydrolysis of borohydride to release an accurate quantity of molecular hydrogen such that the anode is able to oxidize at a given functioning point [99]. For this purpose, they developed Pt–Ni catalysts and claimed that the preliminary results were very promising [100].

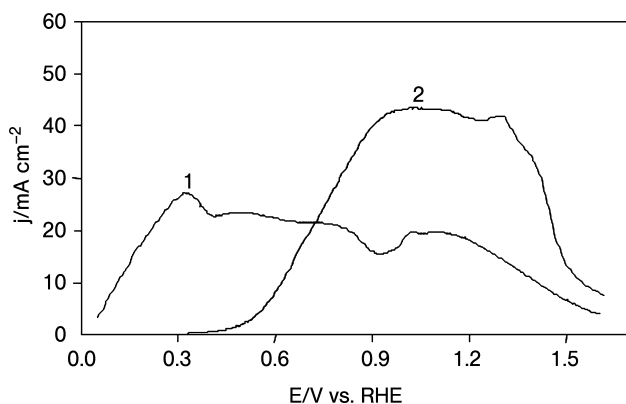


Figure 1.22 Polarization curves for the oxidation of 0.01 M NaBH_4 in a 1 M NaOH solution recorded on (1) Pt (50 wt%)/C and (2) Au (50 wt%)/C; $\nu = 20 \text{ mV s}^{-1}$, $\Omega = 1000 \text{ rpm}$, $T = 20^\circ\text{C}$. Catalysts were prepared according to the ‘water in oil’ microemulsion method.

1.4.3

Cathodic Catalysts in Alkaline Medium

Some electrocatalysts as alternatives to platinum have been studied as active catalysts for the oxygen reduction reaction (ORR) in alkaline media, such as palladium-based catalysts [101], ruthenium-based catalysts [102], iron-porphyrin or phthalocyanine catalysts [103, 104], nickel and cobalt catalysts and nickel–cobalt–spinel catalysts [105–107], and especially manganese oxide-based catalysts [108–113]. In the case of palladium catalysts, the onset of the reduction wave is shifted by 50 mV towards more negative potentials in comparison with platinum electrocatalysts. At the beginning of the reduction wave, water is the main reaction product, whereas at higher cathodic overpotentials, hydrogen peroxide becomes the main reaction product [101]. Ruthenium-based catalysts have shown poor performance in the oxygen reduction reaction because of the oxide film that is formed at the catalyst surface; as a result, the electrode becomes inactive towards oxygen reduction [102]. To achieve good activity and stability towards ORR, iron porphyrins have to be pyrolyzed at about 700 °C. Then, the onset of the reduction wave is close to that obtained with a platinum catalyst. Moreover, the main reaction product remains water, even though some hydrogen peroxide is produced particularly at high overvoltages [103, 104]. The nickel- or cobalt-based electrocatalysts showed poor activity for ORR in alkaline media. Oxygen reduction on these materials occurs only via a two-electron mechanism, producing hydrogen peroxide as the main product. On the other hand, spinel of cobalt and nickel oxides, $\text{Ni}_x\text{Co}_{3-x}\text{O}_4$ ($0 < x < 1$), showed better activity towards ORR, but the reaction mechanism via four electrons is not the main one and a large amount of hydrogen peroxide is formed [105–107]. Manganese oxides have been extensively studied and it was shown that the activity of these catalysts depends on the kind of oxides. The most active were the oxides $\alpha\text{-MnO}_2$, $\gamma\text{-MnO}_2$, Mn_2O_3 and MnOOH [108, 110, 111]. The reaction mechanism on these catalysts involves the formation of the HO_2^- intermediate via the transfer of two electrons followed by a dismutation reaction of this species into OH^- and O_2 . The kinetics of the dismutation reaction is so fast, particularly on the MnOOH catalyst, that apparently four electrons are exchanged during the ORR [109, 113]. Manganese oxides doped with Ni and/or Mg have also been studied in terms of activity towards ORR [41, 112, 113]. It appeared that the use of nickel as doping agent allowed the best activity to be obtained. Indeed, the reduction wave was shifted by 100 mV towards higher potentials and started only 50 mV lower than the reduction wave obtained at a platinum catalyst. However, the mechanism of reaction remains the same as for manganese oxides alone, that is, via the HO_2^- dismutation reaction. Ag-based cathodes have an extensive history with alkaline fuel cells, for example Raney Ag-based cathodes were used by Siemens to develop AFCs for military applications [114]. Moreover, Ag nanoparticles deposited on carbon are very easy to prepare and are known to be active towards the ORR [115].

Demarconnay *et al.* used a method derived from that of the so-called ‘water-in-oil microemulsion’ method to prepare well dispersed Ag/C catalysts [116]. The onset of the oxygen reduction wave is only shifted by 50 mV towards lower potentials on an Ag/C catalyst compared with that obtained on a Pt/C catalyst and the limiting current

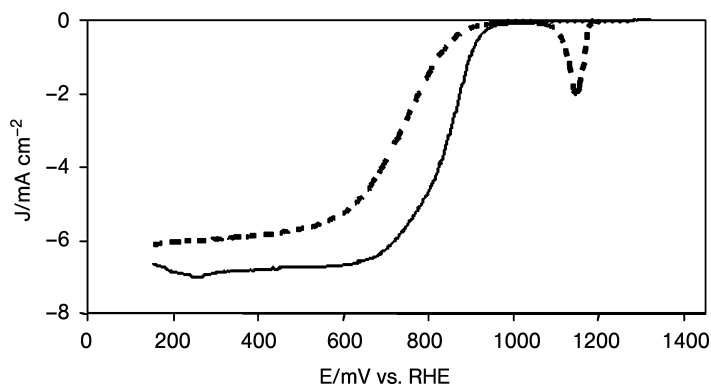


Figure 1.23 $j(E)$ polarization curves recorded at a rotation rate $\Omega = 2500$ rpm in an O_2 -saturated 0.1 M NaOH electrolyte ($T = 20^\circ C$, $\nu = 5 \text{ mV s}^{-1}$) for (dashed line) 20 wt% Ag/C and (solid line) 20 wt% Pt/C. Ag/C catalyst was prepared according to the ‘water-in-oil’ microemulsion method, whereas Pt/C catalyst was prepared using the Bönemann method.

densities are very close for both catalysts (Figure 1.23), indicating that a similar mechanism is involved at least at high overvoltage. On the basis of rotating disk electrode and rotating ring disk electrode experiments, it was shown that nanodispersed Ag particles on carbon powder led to the reduction of molecular oxygen mainly to water, which is similar to the result obtained with platinum (see Table 1.3).

According to the results obtained from rotating ring disk experiments and the determination of Tafel slopes, it was concluded that the mechanism of oxygen electroreduction on an Ag/C catalyst is similar to that on a Pt/C catalyst at high potentials, that is, interesting potentials for fuel cell applications. Lee *et al.* also showed that a 30 wt% Ag electrode displayed the same electroactivity towards the ORR as a 10 wt% electrode and that the activity could be enhanced by doping Ag with Mg [115].

Table 1.3 Total number of exchanged electrons n_t as determined by RDE^b and RRDE^d experiments.

E (V vs RHE)	KL slopes ^a at Pt/C	KL slopes ^a at Ag/C	20 wt% Ag/C				
			n_{RDE}^b	j_D^c (mA cm ⁻²)	$(j_{R,1}^0 - j_{R,1})^c$ (μA cm ⁻²)	n_{RRDE}^d	$p(H_2O)$
0.87	—	—	—	0.121	0	4	100
0.77	6.06	—	—	1.161	0	4	100
0.67	5.91	6.70	3.6	2.735	10.1	3.9	96.4
0.57	6.17	6.76	3.5	3.605	21.6	3.9	94.2
0.47	6.22	6.79	3.5	3.967	34.2	3.8	91.7
0.37	6.07	6.71	3.6	4.236	40.2	3.8	90.9
0.27	6.10	6.60	3.7	4.448	49.2	3.8	89.5

Slopes^a determined from the Koutecky–Levich (KL) plots; j_D and j_R are the disk and ring current densities, respectively^c. $p(H_2O)$ is the fraction of water produced.

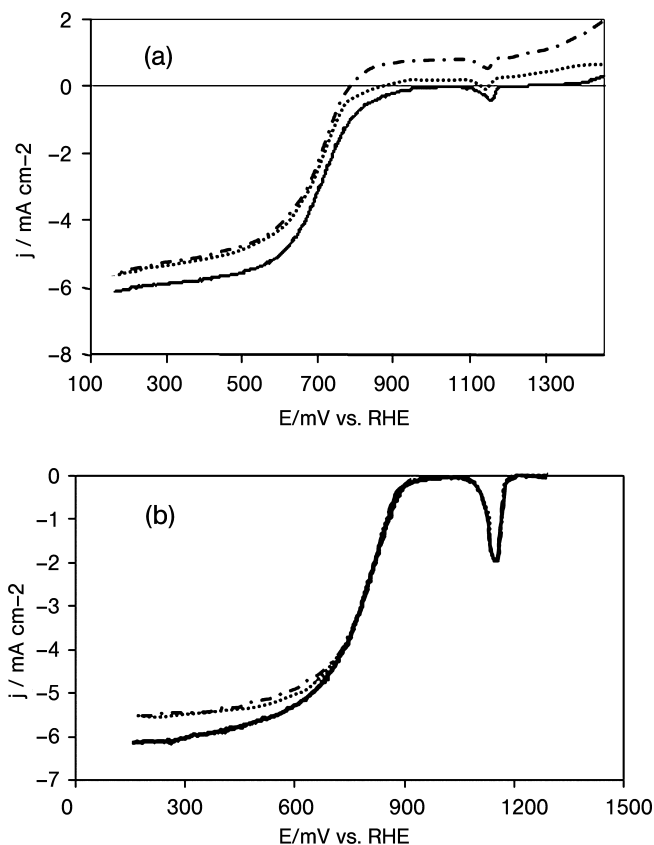


Figure 1.24 $j(E)$ polarization curves recorded on 20wt% Ag/C at a rotation rate $\Omega = 2500$ rpm in an O_2 -saturated 0.1 M NaOH electrolyte in the presence of alcohol ($T = 20^\circ\text{C}$, $\nu = 5$ mVs). (a) (—) Methanol-free electrolyte; (.....) 0.1 M methanol; (-·-·-·) 0.5 M methanol. (b) (—) EG-free electrolyte; (.....) 0.1 M EG; (-·-·-·) 0.5 M EG. Catalysts were prepared according to the ‘water-in-oil’ microemulsion method.

Moreover, for methanol concentrations higher than 0.1 M, the Ag/C cathode catalyst displayed higher tolerance towards methanol than Pt/C (Figure 1.24a) and almost total insensitivity towards the presence of EG (Figure 1.24b).

Other platinum-free materials, such as cobalt and iron macrocycles, display total insensitivity to the presence of methanol [117–119], whereas manganese oxides show very good tolerance towards the presence of NaBH_4 [120]. However, for portable applications, the fuel concentration has to be very high in order to increase the stored energy density and hence the autonomy of the system. Nevertheless, the intrinsic electroactivity of platinum free catalysts being lower than that of platinum, it could be interesting to modify platinum catalysts with foreign metal elements, in order to improve their tolerance towards the presence of the fuel and to increase their electrocatalytic activity towards the ORR. Numerous studies have shown that

platinum-based binary alloyed electrocatalysts such as Pt–Fe, Pt–Co, Pt–Ni and Pt–Cr exhibit in acid electrolytes a higher catalytic activity for the ORR than pure platinum [17, 121–124] and a higher tolerance to the presence of alcohol [18, 125–127]. The observed electrocatalytic enhancement was interpreted either by an electronic factor, that is, the change in the d-band vacancy of Pt upon alloying, and/or geometric effects (Pt coordination number and Pt–Pt distance). Both effects should enhance the reaction rate of oxygen adsorption and the breaking of the O–O bond during the reduction reaction. For example, the lattice parameter a_0 in the case of a cubic Pt–X catalyst ($X = \text{Fe}, \text{Co}, \text{Ni}$) decreases with increasing content of the alloying component X, leading to changes in the catalytic behavior. In the case of Pt–Ni alloys, the maximum electrochemical activity for the ORR is obtained with 30 at.% of Ni [128]. Lemire *et al.* also showed that the presence of highly uncoordinated atoms is very important for CO adsorption at Au nanoparticles [129]. The same effect can also be true for oxygen adsorption at platinum nanoparticles. In addition to electronic, geometric, coordination and size effects, it was also proposed by Shukla *et al.* [130], that foreign metals, such as Cr, can protect platinum from oxidation and hence enhance the electrocatalytic activity of platinum towards the ORR. In alkaline medium, Adžič *et al.* pointed out that the addition of bismuth adatoms to an Au electrode led to greatly enhanced electrocatalytic activity towards the ORR [131].

Demarconnay *et al.* prepared nanodispersed Pt–Bi catalysts with different atomic compositions for the ORR [132]. They showed that a $\text{Pt}_{0.8}\text{Bi}_{0.2}/\text{C}$ catalyst led to a shift of the onset potential of the ORR towards higher potentials together with a higher tolerance towards the presence of EG (Figure 1.25) compared with a pure platinum catalyst. They explained this enhancement in activity and tolerance by the protection of the platinum surface by bismuth oxides. In the potential range where the ORR starts to occur, Bi_2O_5 surface species start to undergo a reduction reaction in Bi_2O_4 , liberating oxide-free sites of platinum by decreasing the coverage by higher oxides of

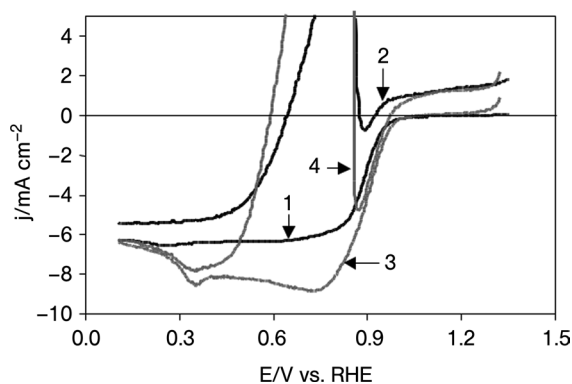


Figure 1.25 $j(E)$ polarization curves for the oxygen reduction reaction recorded in oxygen-saturated 0.2 M NaOH: (1) at Pt/C; (2) at Pt/C in the presence of 0.1 M EG; (3) at $\text{Pt}_{0.8}\text{Bi}_{0.2}/\text{C}$; (4) at $\text{Pt}_{0.8}\text{Bi}_{0.2}/\text{C}$ in the presence of 0.1 M EG ($\nu = 5 \text{ mV s}^{-1}$, $\Omega = 2500 \text{ rpm}$; $T = 20^\circ \text{C}$). Catalysts were prepared according to the ‘water-in-oil’ microemulsion method.

bismuth. The newly accessible oxide-free platinum sites become active for oxygen reduction. Moreover, the liberation of oxide-free platinum sites in a potential range where EG is not expected to adsorb at platinum leads to a higher tolerance of Pt–Bi towards the presence of EG.

1.5

Conclusion

Ethanol is one of the most popular fuels produced from biomass (by fermentation of sugar-containing crops or of numerous agricultural and municipal wastes) and has a relatively high energy density (about two-thirds of that of gasoline and one-quarter of that of pure hydrogen). Its clean and efficient direct conversion into energy then becomes a challenge, particularly its conversion into electricity inside a fuel cell. The development of PEMFCs and more recently of SAMFCs brings new opportunities to the use of ethanol in a direct fuel cell, working either in acidic (PEM) or alkaline (AEM) medium.

In an acidic medium, a PEMFC fed with ethanol allows power densities up to 60 mW cm^{-2} to be reached at high temperatures ($80\text{--}120^\circ\text{C}$), but this needs platinum-based catalysts, which may prevent wider applications for portable electronic devices. On the other hand, in an alkaline medium, the activity of non-noble catalysts for ethanol or ethylene glycol oxidation and oxygen reduction is sufficient to reach power densities of the order of 20 mW cm^{-2} at room temperature. This opens up the hope of developing SAMFCs that are particularly efficient for large-scale portable applications.

References

- Grove, W.R. (1839) *Philosophical Magazine*, **14**, 127–130. Grove, W.R.; (1843) *Journal of the Franklin Institute*, **35**, 277–280.
- Gosselink, J.W. (2002) *International Journal of Hydrogen Energy*, **27**, 1125–1129.
- Ströbel, R., Oszcipok, M., Fasil, M., Rohland, B., Jörissen, L. and Garcke, J. (2002) *Journal of Power Sources*, **105**, 208–215.
- Tilak, B.V., Yeo, R.S. and Srinivasan, S. (1981) *Comprehensive Treatise of Electrochemistry*, Vol. 3 (eds J.O'M. Bockris, B.E. Conway, E. Yeager and R.E. White), Plenum Press, New York, pp. 39–122.
- Appleby, A.J. and Foulkes, F.R. (1989) *Fuel Cell Handbook*, Van Nostrand Reinhold, New York, pp. 203–500.
- Lamy, C. and Léger, J.-M. (1994) *Journal de Physique IV*, **4**, C1, 253–281.
- Kordesch, K. and Simader, G. (1996) *Fuel Cells and Their Applications*, VCH Verlag GmbH, Weinheim.
- Vielstich, W., Lamm, A. and Gasteiger, H. (2003) *Handbook of Fuel Cells: Fundamental, Technology and Applications*, Vol. 1, John Wiley & Sons, Ltd, Chichester.
- Bockris, J.O'M. and Reddy, A.K.N. (1972) *Modern Electrochemistry*, Vol. 2, Plenum Press, New York, p. 1141.
- Sakellaropoulos, G.P. (1981) *Advances in Catalysis*, Vol. 30 (eds D.D. Eley, H. Pines and P.B. Weisz), Academic Press, New York, p. 218.
- Appleby, A.J., Conway, B.E. and Bockris, J.O'M. (1983) *Comprehensive Treatise of*

- Electrochemistry*, Vol. 7 (eds E. Yeager, S.U.M. Khan, R.E. White), Plenum Press, New York, pp. 173–239.
- 12 Krishtalik, L.I. (1970) *Advances in Electrochemistry and Electrochemical Engineering*, Vol. 7 (ed. P. Delahay), Interscience, New York. Trasatti, S. (1972) *Journal of Electroanalytical Chemistry*, **39**, 163–184.
 - 13 Lamy, C., Léger, J.-M., Srinivasan, S. and Bockris, J.O'M. (2001) in *Modern Aspects of Electrochemistry*, Vol. 34 (eds B.E. Conway and R.E. White), Kluwer Academic/Plenum Publishers, New York, pp. 53–118.
 - 14 Watanabe, M. and Motoo, S. (1975) *Journal of Electroanalytical Chemistry*, **60**, 267–273; 275–283.
 - 15 Dubau, L., Coutanceau, C., Garnier, E., Léger, J.-M. and Lamy, C. (2003) *Journal of Applied Electrochemistry*, **33**, 419–429.
 - 16 Tarasevich, M.R., Sadkowski, A. and Yeager, E. (1983) *Comprehensive Treatise of Electrochemistry*, Vol. 7 (eds B.E. Conway, J.O'M. Bockris, E. Yeager, S.U.M. Khan and R.E. White), Plenum Press, New York, pp. 301–398.
 - 17 Ralph, T.R. and Hogarth, M.P., (2002) *Platinum Metals Review*, **46**, 3–14.
 - 18 Yang, H., Alonso-Vante, N., Léger, J.-M. and Lamy, C. (2004) *Journal of Physical Chemistry. B*, **108**, 1938–1947.
 - 19 Stevens, P., Novel-Catin, F., Hammou, A., Lamy, C. and Cassir, M. (2000) *Traité Génie Electrique, D3 340* (ed R. Bonnefille), Techniques de l'Ingénieur, Paris, pp. 1–28.
 - 20 Lamy, C., Kauffmann, J.-M. and Grenier, J.-C. (2003) *Livre Blanc 'Programme ENERGIE du CNRS, Ministère Délégué à la Recherche et aux Nouvelles Technologies*, Paris, pp. 21–41.
 - 21 Jones, D.J., Rozière, J., Marrony, M., Lamy, C., Coutanceau, C., Léger, J.-M., Hutchinson, H. and Dupont, M. (2005) *Fuel Cells Bulletin*, **10**, 12–15.
 - 22 Lamy, C., Belgsir, E.M. and Léger, J.-M. (2001) *Journal of Applied Electrochemistry*, **31**, 799–809.
 - 23 Lamy, C., Lima, A., Le Rhun, V., Delime, F., Coutanceau, C. and Léger, J.-M. (2002) *Journal of Power Sources*, **105**, 283–296.
 - 24 Rousseau, S., Coutanceau, C., Lamy, C. and Léger, J.-M. (2006) *Journal of Power Sources*, **158**, 18–24.
 - 25 Rightmire, R.A., Rowland, R.L., Boos, D.L. and Beals, D.L. (1964) *Journal of the Electrochemical Society*, **111**, 242.
 - 26 Iwasita, T. and Pastor, E. (1994) *Electrochimica Acta*, **39**, 531. Iwasita, T. and Pastor, E. (1994) *Electrochimica Acta*, **39**, 547.
 - 27 Wang, J., Wasmus, S. and Savinell, R.F. (1995) *Journal of the Electrochemical Society*, **142**, 4218.
 - 28 Souza, J., Rabelo, F.J.B., de Moraes, I.R. and Nart, F.C. (1997) *Journal of Electroanalytical Chemistry*, **420**, 17.
 - 29 Hitmi, H. (1992) PhD Thesis, University of Poitiers.
 - 30 Delime, F., Léger, J.-M. and Lamy, C. (1999) *Journal of Applied Electrochemistry*, **29**, 1249.
 - 31 Rezzouk, A. (1994) PhD Thesis, University of Poitiers.
 - 32 Bonarowska, M., Malinowski, A. and Karpinski, Z. (1999) *Applied Catalysis A: General*, **188**, 145.
 - 33 Aboul-Gheit, A.K., Menoufy, M.F. and El-Morsi, A.K. (1990) *Applied Catalysis*, **61**, 283.
 - 34 Hitmi, H., Belgsir, E.-M., Léger, J.-M., Lamy, C. and Lezna, R.O. (1994) *Electrochimica Acta*, **39**, 407.
 - 35 Perez, J.M., Beden, B., Hahn, F., Aldaz, A. and Lamy, C. (1989) *Journal of Electroanalytical Chemistry*, **262**, 251.
 - 36 Lamy, C., Rousseau, S., Belgsir, E.-M., Coutanceau, C. and Léger, J.-M. (2004) *Electrochimica Acta*, **49**, 3901–3908.
 - 37 Vigier, F., Coutanceau, C., Hahn, F., Belgsir, E.M. and Lamy, C. (2004) *Journal of Electroanalytical Chemistry*, **563**, 81–89.
 - 38 Liu, P., Logadottir, A. and Nørskov, J.K. (2003) *Electrochimica Acta*, **48**, 3731.
 - 39 Morimoto, Y. and Yeager, E.B. (1998) *Journal of Electroanalytical Chemistry*, **441**, 77.

- 40 Shubina, T.E. and Koper, M.T.M. (2002) *Electrochimica Acta*, **47**, 3621.
- 41 Yang, C.-C. (2004) *International Journal of Hydrogen Energy*, **29**, 135–143.
- 42 Wang, Y., Li, L., Hu, L., Zhuang, L., Lu, J. and Xu, B. (2003) *Electrochemistry Communications*, **5**, 662–666.
- 43 Iwamoto, T., Uetake, M. and Umeda, A. (1994) Hofman degradation of strong base anion exchange resin, Proceedings of the 68th Autumn Annual Meeting of the Chemical Society of Japan, Nagoya October 1994, p.472.
- 44 Matsui, K., Tobita, E., Sugimoto, K., Kondo, K., Seita, T. and Akimoto, A. (1986) *Journal of Applied Polymer Science*, **32**, 4137–4143.
- 45 Hunger, H.F. (1960) Proceedings of the Annual Power Sources Conference, Vol. 14, p.55.
- 46 Sata, T., Tsujimoto, M., Yamaguchi, T. and Matsusaki, K. (1996) *Journal of Membrane Science*, **112**, 161–170.
- 47 Fang, J. and Shen, P.K. (2006) *Journal of Membrane Science*, **285**, 317–322.
- 48 Li, L., Zhang, J. and Wang, Y.X. (2003) *Journal of Membrane Science*, **226**, 159–167.
- 49 Li, L. and Wang, Y.X. (2005) *Journal of Membrane Science*, **262**, 1–4.
- 50 Yu, E.H. and Scott, K. (2004) *Journal of Power Sources*, **137**, 248–256.
- 51 Coutanceau, C., Demarconnay, L., Léger, J.-M. and Lamy, C. (2006) *Journal of Power Sources*, **156**, 14–19.
- 52 Demarconnay, L., Brimaud, S., Coutanceau, C. and Léger, J.-M. (2007) *Journal of Electroanalytical Chemistry*, **601**, 169–180.
- 53 Varcoe, J.R., Slade, R.C.T., Yee, E.L.H., Poynton, S.D. and Driscoll, D.J. (2007) *Journal of Power Sources*, **173**, 194–199.
- 54 Varcoe, J.R. and Slade, R.C.T. (2006) *Electrochemistry Communications*, **8**, 839–843.
- 55 Slade, R.C.T. and Varcoe, J.R. (2005) *Solid State Ionics*, **176**, 585–597.
- 56 Herman, H. Slade, R.C.T. and Varcoe, J.R. (2003) *Journal of Membrane Science*, **218**, 147–163.
- 57 Hübner, G. and Roduner, E. (1999) *Journal of Materials Chemistry*, **9**, 409–418.
- 58 Matsuoka, K., Iriyama, Y., Abe, T., Matsuoka, M. and Ogumi, Z. (2005) *Journal of Power Sources*, **150**, 27–31.
- 59 Agel, E., Bouet, J. and Fauvarque, J.F. (2001) *Journal of Power Sources*, **101**, 267–274.
- 60 Stoica, D., Ogier, L., Akrouer, L. and Alloin, F. Fauvarque, J.-F. (2007) *Electrochimica Acta*, **53**, 1596–1603.
- 61 Schiedaa, M., Roualdès, S., Durand, J., Martinent, A. and Marsacq, D. (2006) *Desalination*, **199**, 286–288.
- 62 Varcoe, J.R. and Slade, R.C.T. (2005) *Fuel Cells*, **5**, 187–200.
- 63 Yang, C.-C., Chiu, S.-J. and Chien, W.-C. (2006) *Journal of Power Sources*, **162**, 21–29.
- 64 Yang, C.-C. (2007) *Journal of Membrane Science*, **288**, 51–60.
- 65 Xing, B. and Savadogo, O. (2000) *Electrochemistry Communications*, **2**, 697–702.
- 66 Kordesch, K.V. (1978) *Journal of the Electrochemical Society*, **125**, 77C–88C.
- 67 Kirov, Y. and Schwartz, S. (2000) *Journal of Power Sources*, **87**, 101–105.
- 68 Ewe, H., Justi, E. and Schmitt, A. (1974) *Electrochimica Acta*, **19**, 799–808.
- 69 Mund, K., Richter, G. and Von Sturm, F. (1977) *Journal of the Electrochemical Society*, **125**, 1–6.
- 70 Kenjo, T. (1985) *Journal of the Electrochemical Society*, **132**, 383–386.
- 71 Vigier, F., Rousseau, S., Coutanceau, C., Léger, J.-M. and Lamy, C. (2006) *Topics in Catalysis*, **40**, 111–121.
- 72 Song, S. and Tsiakara, P. (2006) *Applied Catalysis B: Environmental*, **63**, 187–193.
- 73 Frelink, T., Visscher, W. and Van Veen, J.A.R. (1996) *Langmuir*, **12**, 3702–3708.
- 74 Matsuoka, K., Iriyama, Y., Abe, T., Matsuoka, M. and Ogumi, Z. (2005) *Electrochimica Acta*, **51**, 1085–1090.

- 75 Ewe, H., Justi, E. and Pesditschek, M. (1975) *Energy Conversion*, **15**, 9–14.
- 76 Hauffe, W. and Heitbaum, J. (1978) *Electrochimica Acta*, **23**, 299–304.
- 77 Santos, E. and Giordano, M.C. (1985) *Electrochimica Acta*, **30**, 871–878.
- 78 Kadirgan, F., Bouhier-Charbonnier, E., Lamy, C., Léger, J.-M. and Beden, B. (1990) *Journal of Electroanalytical Chemistry*, **286**, 41–61.
- 79 de Lima, R.B., Paganin, V., Iwasita, T. and Vielstich, W. (2003) *Electrochimica Acta*, **49**, 85–91.
- 80 Dalbay, N. and Kadirgan, F. (1990) *Journal of Electroanalytical Chemistry*, **296**, 559–569.
- 81 Pattabiraman, R. (1997) *Applied Catalysis A: General*, **153**, 9–20.
- 82 Beden, B., Kadirgan, F., Kahyaoglu, A. and Lamy, C. (1982) *Journal of Electroanalytical Chemistry*, **135**, 329–334.
- 83 Smirnova, N.W. Petrii, O.A. and Grzejdzia, A. (1988) *Journal of Electroanalytical Chemistry*, **251**, 73–87.
- 84 Kadirgan, F., Beden, B. and Lamy, C. (1982) *Journal of Electroanalytical Chemistry*, **136**, 119–138.
- 85 Kadirgan, F., Beden, B. and Lamy, C. (1983) *Journal of Electroanalytical Chemistry*, **143**, 135–152.
- 86 Knobloch, H., Gröppel, D., Kohlmüller, H., Kühl, D. and Siemsen, G. (1979) in *Power Sources 7. Proceedings of the 11th Symposium, Brighton, 1978, Vol. 24* (ed. J. Thomson), Academic Press, London, p. 389.
- 87 Xu, C., Cheng, L., Shen, P.K. and Liu, Y. (2007) *Electrochemistry Communications*, **9**, 997–1001.
- 88 Shen, P.K. and Xu, C. (2006) *Electrochemistry Communications*, **8**, 184–188.
- 89 Bert, P. and Bianchini, C. (2006) Platinum-free electrocatalysts materials, European Patent EP 1 556 916 B1.
- 90 Bert, P., Bianchini, C., Giambastiani, G., Miller, H., Santiccioli, S., Tampucci, A. and Vizza, F. (2006) Direct fuel cells comprising a nitrogen compounds and their use, Republica Italiana Dom. It. FI2006A000160.
- 91 Bert, P., Bianchini, C., Emiliani, C., Giambastiani, G., Santiccioli, S., Tampucci, A. and Vizza, F. (2006) Anode catalysts made of noble metal spontaneously deposited onto nanostructured catalysts based on transition metals, their preparation and use and fuel cells containing them, Republica Italiana Dom. It. FI2006A000180.
- 92 Amendola, S.C., Onnerud, P., Kelly, M.T., Petillo, P.J., Sharp-Goldman, S.L. and Binder, M. (1999) *Journal of Power Sources*, **84**, 130–133.
- 93 Li, Z.P., Liu, B.H., Arai, K., Asaba, K. and Suda, S. (2004) *Journal of Power Sources*, **126**, 28–33.
- 94 Mirkin, M.V. Yang, H. and Bard, A.J. (1992) *Journal of the Electrochemical Society*, **139**, 2212–2217.
- 95 Elder, J.P. and Hickling, A. (1962) *Transactions of the Faraday Society*, **58**, 1852–1864.
- 96 Liu, B.H., Li, Z.P., Arai, K. and Suda, S. (2005) *Electrochimica Acta*, **50**, 3719–3725.
- 97 Li, Z.P., Liu, B.H., Arai, K. and Suda, S. (2005) *Journal of Alloys and Compounds*, **404–406**, 648–652.
- 98 Chatenet, M., Micoud, F., Roche, I. and Chainet, E. (2006) *Electrochimica Acta*, **51**, 5459–5467.
- 99 Jamard, R., Latour, A., Salomon, J., Capron, P. and Martinet-Beaumont, A. (2008) *Journal of Power Sources*, **176**, 287–292.
- 100 Latour, A. (2006) PhD Thesis, Institut National Polytechnique de Grenoble.
- 101 Yang, Y.-F., Zhou, Y.-H. and Cha, C.-S. (1995) *Electrochimica Acta*, **40**, 2579–2586.
- 102 Prakash, J. and Joachin, H. (2000) *Electrochimica Acta*, **45**, 2289–2296.
- 103 Gojkovic, S.L., Gupta, S. and Savinell, R.F. (1999) *Journal of Electroanalytical Chemistry*, **462**, 63–72.
- 104 Gojkovic, S.L., Gupta, S. and Savinell, R.F. (2000) *Electrochimica Acta*, **45**, 889–897.

- 105 Heller-Ling, N. Prestat, M. Gautier, J.-L. and Koenig, J.-F. (1997) *Electrochimica Acta*, **42**, 197–202.
- 106 Hu, Y., Tolmachev, Y.V. and Scherson, D.A. (1999) *Journal of Electroanalytical Chemistry*, **468**, 64–69.
- 107 Rashkova, V., Kitova, S., Konstantinov, I. and Vitanov, T. (2002) *Electrochimica Acta*, **47**, 1555–1560.
- 108 Ponce, J., Rehspringer, J.-L., Poillierat, G. and Gautier, J.-L. (2001) *Electrochimica Acta*, **46**, 3373–3380.
- 109 Matsuki, K. and Kamada, H. (1986) *Electrochimica Acta*, **31**, 13–18.
- 110 Mao, L., Sotomura, T., Nakatsu, K., Koshihara, N., Zhang, D. and Ohsaka, T. (2002) *Journal of the Electrochemical Society*, **149**, A504–A507.
- 111 Klapste, B., Vondrak, J. and Velicka, J. (2002) *Electrochimica Acta*, **47**, 2365–2369.
- 112 Yang, J. and Xu, J.J. (2003) *Electrochemistry Communications*, **5**, 306–311.
- 113 Mao, L., Zhang, D., Sotomura, T., Nakatsu, K., Koshihara, N. and Ohsaka, T. (2003) *Electrochimica Acta*, **48**, 1015–1021.
- 114 Strasser, K. (2003) in *Handbook of Fuel Cells – Fundamentals, Technology and Applications*, Vol. 4 (eds W. Vielstich, H.A. Gasteiger and A. Lamm), John Wiley & Sons, Ltd, Chichester, p. 775.
- 115 Lee, H.-K., Shim, J.-P., Shim, M.-J., Kim, S.-W. and Lee, J.-S. (1996) *Materials Chemistry and Physics*, **45**, 238–242.
- 116 Demarconnay, L., Coutanceau, C. and Léger, J.-M. (2004) *Electrochimica Acta*, **49**, 4513–4521.
- 117 Convert, P., Coutanceau, C., Crouigneau, P., Gloaguen, F. and Lamy, C. (2001) *Journal of Applied Electrochemistry*, **31**, 945–952.
- 118 Baranton, S., Coutanceau, C., Roux, C., Hahn, F. and Léger, J.-M. (2005) *Journal of Electroanalytical Chemistry*, **577**, 223–234.
- 119 Zagal, J.H. (2003) in *Handbook of Fuel Cells – Fundamental, Technology and Applications*, Vol. 1 (eds W. Vielstich, A. Lamm and H.A. Gasteiger), John Wiley and Sons, Ltd, Chichester, pp. 544–554.
- 120 Chatenet, M., Micoud, F., Roche, I., Chainet, E. and Vondrak, J. (2006) *Electrochimica Acta*, **51**, 5452–5458.
- 121 Paffet, M.T., Beery, J.G. and Gottesfeld, S. (1988) *Journal of the Electrochemical Society*, **135**, 1431–1436.
- 122 Beard, B.C. and Ross, P.N. (1990) *Journal of the Electrochemical Society*, **137**, 3368–3374.
- 123 Toda, T., Igarashi, H. and Watanabe, M. (1999) *Journal of Electroanalytical Chemistry*, **460**, 258–262.
- 124 Neergat, N., Shukla, A. and Gandhi, K.S. (2001) *Journal of Applied Electrochemistry*, **31**, 373–378.
- 125 Ralph, T.R. and Hogarth, M.P. (2002) *Platinum Metals Review*, **46**, 146–164.
- 126 Yang, H., Coutanceau, C., Léger, J.-M., Alonso-Vante, N. and Lamy, C. (2005) *Journal of Electroanalytical Chemistry*, **576**, 305–313.
- 127 Koffi, R.C., Coutanceau, C., Garnier, E., Léger, J.-M. and Lamy, C. (2005) *Electrochimica Acta*, **50**, 4117–4127.
- 128 Toda, T., Igarashi, H., Uchida, H. and Watanabe, M. (1999) *Journal of the Electrochemical Society*, **146**, 3750–3756.
- 129 Lemire, C. Meyer, R. Shaikhutdinov, S. and Freund, H.-J. (2003) *Angewandte Chemie International Edition*, **43**, 118–121.
- 130 Shukla, A., Neergat, M., Parthasarathi, B., Jayaram, V. and Hegde, M.S. (2001) *Journal of Electroanalytical Chemistry*, **504**, 111–119.
- 131 Adžič, R.R. (1984) *Advances in Electrochemistry and Electrochemical Engineering*, Vol. 13 (eds H. Gerisher and C.W. Tobias) Wiley-Interscience, New York, p 159.
- 132 Demarconnay, L., Coutanceau, C. and Léger, J.-M. (2008) *Electrochimica Acta*, **53**, 3232–3241.